

## Further Study on Errors in Metric Evaluation by Linear Upwind Schemes with Flux Splitting in Stationary Grids

Qin Li<sup>1,2,\*</sup>, Dong Sun<sup>1</sup> and Pengxin Liu<sup>1</sup>

<sup>1</sup> State Key Laboratory of Aerodynamics, Mianyang, Sichuan, 621000, P.R. China.

<sup>2</sup> National Laboratory of Computational Fluid Dynamics, Beijing University of Aeronautics and Astronautics, Beijing 100191, P.R. China.

Communicated by Kun Xu

Received 29 July 2016; Accepted (in revised version) 10 January 2017

---

**Abstract.** The importance of eliminating errors in grid-metric evaluation for high-order difference schemes has been widely recognized in recent years, and it is known from the proof by Vinokur and Yee (NASA TM 209598, 2000) that when conservative derivations of grid metric are used by Thomas, Lombard and Neier (AIAA J., 1978, 17(10) and J. Spacecraft and rocket, 1990, 27(2)), errors caused by metric evaluation could be eliminated by linear schemes when flux splitting is not considered. According to the above achievement, central schemes without the use of flux splitting could fulfill the requirement of error elimination. Difficulties will arise for upwind schemes to attain the objective when the splitting is considered. In this study, further investigations are made on three aspects: Firstly, an idea of central scheme decomposition is introduced, and the procedure to derive the central scheme is proposed to evaluate grid metrics only. Secondly, the analysis has been made on the requirement of flux splitting to acquire free-stream preservation, and a Lax-Friedrichs-type splitting scheme is proposed as an example. Discussions about current study with that by Nonomura et al. (Computers and Fluids, 2015, 107) have been made. Thirdly, for half-node- or mixed-type schemes, interpolations should be used to derive variables at half nodes. The requirement to achieve metric identity on this situation is analyzed and an idea of directionally consistent interpolation is proposed, which is manifested to be indispensable to avoid violations of metric identity and to eliminate metric-caused errors thereafter. Two numerical problems are tested, i.e., the free-stream and vortex preservation on wavy, largely randomized and triangular-like grids. Numerical results validate aforementioned theoretical outcomes.

**AMS subject classifications:** 65M06

**Key words:** Upwind scheme, flux splitting, metric identity, free-stream preservation.

---

\*Corresponding author. *Email addresses:* qin-li@vip.tom.com (Q. Li), sund1986@foxmail.com (D. Sun), liupengxin2008@163.com (P. Liu)

## 1 Introduction

It is well-known in computational fluid dynamics (CFD) that the use of deformed grids usually leads to unsatisfactory results. In Ref. [1], Visbal and Gaitonde demonstrated considerable errors might be caused by metric evaluations when using high-order schemes. Later, the numerical investigations by Nonomura, Lizuka and Fujii [2] again verified the importance of the metric computation. Through their work, the issue regarding metric-caused errors has re-gained the attention of CFD community.

At least in 1974, Vinokur [3] gave the conservative forms of Euler Equations in stationary curvilinear coordinate systems, which implied the use of theoretically zero-valued terms, i.e., metric identities. In 1978, Pulliam and Steger [4] pointed out that the presumed zero-valued identities might actually have non-zero value in computations. Hence when the uniform flow condition is imposed, the flow field might change and so-called free-stream preservation (*FSP*) property could be broken. In the following, a brief discussion is made on the efforts to eliminate errors generated in metric evaluations in three aspects:

(1) The form of grid metric. In CFD textbooks, grid metrics are usually expressed in products of coordinate derivatives, e.g.,  $\hat{\xi}_x = y_\eta z_\zeta - z_\eta y_\zeta$ . When this form is chosen, it seems that only second-order schemes with averaging technique [4] can achieve metric cancellation and make metric identity (*MI*) established. Using simple re-combination, Thomas and Lombard [5, 6] proposed a "conservative" form of the metrics, through which the restriction of using specific difference scheme to achieve metric cancellation was largely released. Thomas and Neier [7] further recast the conservative form into a more symmetric one, which later was referred by Vinokur and Yee [8] as the "coordinate invariant form".

(2) The practice of using the same scheme for the metric and flux derivatives in fluid governing equations. In Ref. [9], Thompson et al. mentioned that it would be better to use the same difference representation to evaluate the metric coefficients and the function such as flux derivatives. Gaitonde and Visbal [10] explicitly stated that metrics "computed with the same scheme as employed for the fluxes" could reduce "the error on stretched meshes".

(3) The approaches to avoid errors lead by grid metrics. After numerically testing various center schemes with orders from the second to sixth, Gaitonde and Visbal [10] found the coupling of the same-scheme practice with the conservative form of metrics in Ref. [6] could reduce metric-caused errors to machine zero. Vinokur and Yee [8] realized the key lay in the numerical commutativity of the mixed partial derivative and showed an analytic proof on the commutativity by using the notion of tensor product. Later, different analyses were conducted on the same subject from different aspects [11–14]. Besides the above methods, other efforts were observed such as positively removing the errors introduced during the equation transformations. This idea could be found in Ref. [9] and [15], and Cai and Ladeinde [16] showed a numerical practice of this regard. It is usually suspected whether such practice would be a thorough solution to the problem.

One of the outcomes of the third aspect is that linear central schemes could make *MI* valid when combined with the conservative metrics, e.g., the node- or half-node-type compact schemes by Lele [17]. As shown in Ref. [1], due to zero dissipation, central schemes cannot work independently in practical problems unless combined with the filters for usage. Naturally, it is of interest to know if upwind schemes could eliminate metric-caused errors in stationary grids as well. Thompson et al. [9] indicated complexities would arise from the flux splitting, which was necessary in upwind schemes. It was once doubted if upwind schemes could achieve the purpose of error elimination [2, 11]. In Ref. [23], Nonomura et al. worked on the fifth- and sixth-order WENO schemes and transformed the original  $h_{j+1/2}$  in  $\frac{\partial \hat{f}}{\partial \xi} = \frac{h_{j+1/2} - h_{j-1/2}}{\Delta \xi}$  into a central consistent part plus two nonlinear dissipation parts. In addition, a frozen treatment of grid metric was used in the flux splitting. Combining proposed techniques with the metric derivation by Thomas et al. [6, 7], the modified WENO schemes were shown to keep *FSP* [23]. The authors of this paper had also studied this problem independently. Noticing the connection between a linear upwind scheme and its downwind counterpart, they devised an operation to derive the central scheme for arbitrary linear upwind scheme, and worked out an analogous treatment for flux splitting. Their work will be reported in this study and the discussion on the work with that of Ref. [23] will be given.

While above attempts aim for node-type linear schemes to eliminate errors in metric evaluation, extra problems arise for half-node- or mixed-type schemes. For such schemes, variables at cell edges needed by the scheme are unknown straightforwardly, which should be derived by techniques like interpolation. It seems that available guidelines are only suggestions [9] lacking theoretical analysis. As shown in Section 4, if interpolations are not treated properly, *MI* can still be violated even if aforementioned methods are followed.

Based on the above considerations, further investigation for linear upwind schemes with flux spitting is made to achieve metric cancellation and eliminate related errors. Relevant studies are first reviewed in Section 2. In Section 3, analyses and corresponding methods are introduced for linear upwind schemes to achieve the above purposes. In Section 4, a study on interpolation is made for half-node- or mixed-type schemes. In Section 5, numerical validations are provided to show the validity of the proposed methods. At last, conclusions are drawn in Section 6. Although the above investigations mainly concern linear upwind schemes, the outcomes should be directly applied to low-speed compressible problems and provide foundations for further nonlinear algorithms.

## 2 Metric identities, free-stream preservation and evaluations of grid metrics and Jacobian

### 2.1 Metric identities and free-stream preservation

In this section, two basic terminologies, metric identity and free-stream preservation, are reviewed and their interrelation are referred. Consider the non-dimensional Navier-

Stokes equation in the Cartesian coordinate system

$$\partial_t Q + \partial_x(E - E_v) + \partial_y(F - F_v) + \partial_z(G - G_v) = 0, \quad (2.1)$$

where  $Q = (\rho, \rho u, \rho v, \rho w, e)$  and  $e = \frac{p}{\gamma-1} + \frac{1}{2}\rho(u^2 + v^2 + w^2)$ , and where  $(E, F, G)$  and  $(E_v, F_v, G_v)$  are inviscid and viscous fluxes respectively. The definitions of fluxes are easily found in CFD books and will not be repeated here. For a uniform flow, all spatial derivatives in Eq. (2.1) should be zero and  $Q$  will not change. Hence, the property of free-stream preservation is naturally established.

To solve Eq. (2.1) in the stationary curvilinear coordinates system, the grid transformation is employed:  $(x, y, z) \rightarrow (\xi, \eta, \zeta)$ . For simplicity, some convention of the tensor analysis will be used as:  $\hat{\xi}^j$  denotes  $(\xi, \eta, \zeta)$ ,  $x_i$  denotes  $(x, y, z)$ , and  $u^i$  denotes  $(u, v, w)$ . Using the chain law  $\partial_{x_i} = \hat{\xi}_{x_i}^j \cdot \partial_{\hat{\xi}^j}$ , Eq. (2.1) becomes

$$\partial_t \hat{Q} + \partial_{\hat{\xi}}(\hat{E} - \hat{E}_v) + \partial_{\hat{\eta}}(\hat{F} - \hat{F}_v) + \partial_{\hat{\zeta}}(\hat{G} - \hat{G}_v) = -(\hat{E} - \hat{E}_v, \hat{F} - \hat{F}_v, \hat{G} - \hat{G}_v) \cdot \vec{I}. \quad (2.2)$$

In the equation,  $\hat{Q} = J^{-1}Q$  with  $J^{-1} = \left| \frac{\partial(x, y, z)}{\partial(\xi, \eta, \zeta)} \right|$ ,  $\hat{E} = (\hat{\xi}_x E + \hat{\xi}_y F + \hat{\xi}_z G)$  with  $\hat{\xi}_{x_i}^j = J^{-1} \hat{\xi}_{x_i}^j$ , and  $\hat{F}$ ,  $\hat{G}$ ,  $\hat{E}_v$ ,  $\hat{F}_v$ ,  $\hat{G}_v$  can be derived similarly;  $\vec{I}$  stands for a vector  $(I_x, I_y, I_z)$  with the component as

$$I_{x_i} = (\hat{\xi}_{x_i})_{\hat{\xi}} + (\hat{\eta}_{x_i})_{\hat{\eta}} + (\hat{\zeta}_{x_i})_{\hat{\zeta}} \equiv (\hat{\xi}_{x_i}^j)_{\hat{\xi}^j}. \quad (2.3)$$

Using the notation  $(\cdot)_{\vec{r}} = (\partial_x, \partial_y, \partial_z)$ ,

$$\hat{\xi}_{\vec{r}}^i = \vec{r}_{\hat{\xi}^i} \times \vec{r}_{\hat{\xi}^k}, \quad (2.4)$$

where indices  $(i, j, k)$  are cyclic. It is worth noticing that outside derivatives in Eq. (2.3) like  $(\cdot)_{\hat{\xi}^j}$  come from derivatives imposed on fluxes in Eq. (2.2), while derivatives inside  $\hat{\xi}_{\vec{r}}^i$  in Eq. (2.4) originate from metric computations. It is trivial that due to the commutativity of partial differential derivatives,  $\vec{I} = 0$  or the metric identity holds, and the popular conservative form will be established by discarding the right-hand side term of Eq. (2.2). If the differential  $\partial$  is evaluated by a difference operator  $\delta$ , Eq. (2.2) can be further written as

$$\partial_t \hat{Q} + \delta_{\hat{\xi}}(\hat{E} - \hat{E}_v) + \delta_{\hat{\eta}}(\hat{F} - \hat{F}_v) + \delta_{\hat{\zeta}}(\hat{G} - \hat{G}_v) = 0, \quad (2.5)$$

which is the most common choice employed by simulations. When the uniform-flow condition is imposed, the following equation is sometimes referred [11]:

$$\partial_t \hat{Q} + (E_{\infty}, F_{\infty}, G_{\infty}) \cdot \vec{I}^* - (E_{v, \infty}, F_{v, \infty}, G_{v, \infty}) \cdot \vec{I}^* = 0, \quad (2.6)$$

where  $\vec{I}^*$  is the numerical evaluation of  $\vec{I}$  by replacing  $\partial$  with  $\delta$  correspondingly, and the subscript " $\infty$ " denotes the uniform-flow state. From Eq. (2.6), the establishment of FSP ( $\hat{Q} \equiv \hat{Q}_{\infty}$ ) seems to be equal to the establishment of MI, which is consistent to the discard of  $\vec{I}$  in Eq. (2.2). Due to this, the achievement of MI is seriously concerned by studies.

However, when the flux splitting is considered, Eq. (2.6) usually cannot be attained when using general numerical schemes, therefore, the only numerical validity of *MI* does not guarantee *FSP*. Further discussion in this regard will be continued in Section 3.1.

It should be pointed out that when moving grids are considered, the grid transformation will become  $(x, y, z, t) \rightarrow (\xi, \eta, \zeta, \tau)$ , and extra complexity will arise. In such situation, the achievement of a conservative relation  $(J^{-1})_{\tau} + (\hat{\xi}_t)_{\xi} + (\hat{\eta}_t)_{\eta} + (\hat{\zeta}_t)_{\zeta} = 0$  which is initially called as "geometric conservation law" [5, 6], should be especially concerned. Because current study only regards stationary grids, the issue aroused from moving grids will not be involved.

## 2.2 Evaluation of metrics to achieve metric identities

As discussed, the achievement of metric identities are critical to eliminate metric-caused errors, while the form of grid metrics is of key position in the achievement. It has been indicated in Ref. [5, 10] that the original form of  $\hat{\zeta}_{\vec{r}}^i$  by Eq. (2.4) is hard to achieve *MI* when using ordinary schemes, especially the high-order ones. Using the production rule of derivatives, Thomas and Lombard [5] first proposed the equivalent conservative form as:

$$\hat{\zeta}_{x_{j'}}^i = \left[ (x_{j'})_{\zeta^j} \cdot x_{k'} \right]_{\zeta^k} - \left[ (x_{j'})_{\zeta^k} \cdot x_{k'} \right]_{\zeta^j}, \quad (2.7)$$

where two sets of indices with and without primes are cyclic. Replacing Eq. (2.4) with Eq. (2.7), it was found that  $\vec{I}$  could "vanish identically when central difference operators are used to evaluate the spatial derivatives" [5]. Besides, it can be seen that the positions of  $x_{j'}$  and  $x_{k'}$  in Eq. (2.7) are not equal. Possibly having noticed this unbalance, Thomas and Neier [7] further proposed the symmetric form:

$$\hat{\zeta}_{\vec{r}}^i = \frac{1}{2} \left[ \left( \vec{r} \times \vec{r}_{\zeta^k} \right)_{\zeta^j} + \left( \vec{r}_{\zeta^j} \times \vec{r} \right)_{\zeta^k} \right], \quad (2.8)$$

which is actually the average of Eq. (2.7) and its reciprocal:  $\left[ (x_{k'})_{\zeta^k} \cdot x_{j'} \right]_{\zeta^j} - \left[ (x_{k'})_{\zeta^j} \cdot x_{j'} \right]_{\zeta^k}$ .

It is obvious that when Eq. (2.7) is used to evaluate the grid metric  $\hat{\zeta}_{x_{j'}}^k$ , the second term of the equation will be  $-\left[ (x_{j'})_{\zeta^j} \cdot x_{k'} \right]_{\zeta^i}$ , and its partial derivative with  $\zeta^k$  will cancel out the partial derivative of the first term in  $\hat{\zeta}_{x_{j'}}^i$  with  $\zeta^i$  by considering the commutativity  $\partial_{\zeta^j \zeta^k} = \partial_{\zeta^k \zeta^j}$ . Using similar operations, *MI* will be established through metric cancellations. The conclusion also holds for the use of Eq. (2.8). If the commutativity is also maintained by difference schemes or  $\delta_{\zeta^j \zeta^k} = \delta_{\zeta^k \zeta^j}$ , *MI* should be numerically achieved. In this regard, Vinokur and Yee [8] first gave a proof which will be reviewed in Appendix for brevity. As mentioned in Ref. [8], the proof stands for compact or non-compact schemes, and arbitrary boundary conditions can be incorporated as well. Another implication in the proof is that the difference scheme such as  $\delta_{\zeta}$  or  $\delta_{\eta}$  is constant and consistent in the evaluation of  $(\cdot)_{\zeta^j}$  and  $(\cdot)_{\eta^j}$ . The CFD interpretation of the usage can be further expressed as:

to achieve commutativity, the scheme in each coordinate direction should be linear and keep the same form for the metrics and flux approximation.

When the type of schemes are confined to finite difference, more concise proofs are observed [11, 18], and their main points are reviewed as follows. Without losing generality, suppose the difference operators  $\delta_{\xi}$  and  $\delta_{\eta}$  at  $(i, j, k)$  can be expressed as:

$$\begin{cases} \delta_{\xi}(\cdot)_{i,j,k} = \frac{1}{\Delta} \sum_{i_1=-m_1}^{n_1} a_{i_1}^{\xi}(\cdot)_{i+i_1,j,k}, \\ \delta_{\eta}(\cdot)_{i,j,k} = \frac{1}{\Delta} \sum_{j_1=-m_2}^{n_2} a_{j_1}^{\eta}(\cdot)_{i,j+j_1,k}, \end{cases} \quad (2.9)$$

where  $\Delta$  denotes spatial interval, then for any function  $f_{i,j,k}$

$$\begin{aligned} \delta_{\xi\eta}(f)_{i,j,k} &= \frac{1}{\Delta^2} \sum_{j_1=-m_2}^{n_2} a_{j_1}^{\eta} \left( \sum_{i_1=-m_1}^{n_1} a_{i_1}^{\xi}(f)_{i+i_1,j+j_1,k} \right) \\ &= \frac{1}{\Delta^2} \sum_{i_1=-m_1}^{n_1} a_{i_1}^{\xi} \left( \sum_{j_1=-m_2}^{n_2} a_{j_1}^{\eta}(f)_{i+i_1,j+j_1,k} \right) = \delta_{\eta\xi}(f)_{i,j,k}. \end{aligned}$$

In the formula, the trivial algebraic commutativity of summation is used.

It is worth noticing that only the consistent use of the linear scheme is required in the above proofs, especially when upwind ones are included and schemes can be different in different coordinate directions. In practical applications, the flux will be split into positive and negative parts, and the upwind scheme will evolve into the upwind and downwind parts correspondingly. In this sense, the establishment of *MI* by the individual use of the upwind or downwind scheme does not guarantee *FSP* naturally.

### 2.3 Suggestions for Jacobian evaluation

It was reported in literatures [12, 19] that different forms of  $J^{-1}$  might influence the level of grid-generated errors on seriously deforming grids although they are not related with *MI*. The ordinary definition is:

$$J^{-1} \equiv \left| \frac{\partial(x,y,z)}{\partial(\xi,\eta,\zeta)} \right| = \vec{r}_{\xi i} \cdot (\vec{r}_{\xi j} \times \vec{r}_{\xi k}), \quad (2.10)$$

where the indices are cyclic. If terms like  $\vec{r}_{\xi i}$  are computed individually, the circulation of indices in Eq. (2.10) will not result in different values of  $J^{-1}$ . Considering Eq. (2.4),  $J^{-1}$  can apparently be also expressed as  $\vec{r}_{\xi} \cdot \hat{\zeta}_{\vec{r}}$ , which might be numerically different to  $\vec{r}_{\xi} \cdot \hat{\zeta}_{\vec{r}}$  or  $\vec{r}_{\eta} \cdot \hat{\eta}_{\vec{r}}$ . So if  $\hat{\zeta}_{\vec{r}}$  is evaluated by Eq. (2.7) or (2.8),  $\vec{r}_{\xi} \cdot \hat{\zeta}_{\vec{r}}$ ,  $\vec{r}_{\eta} \cdot \hat{\eta}_{\vec{r}}$  and  $\vec{r}_{\zeta} \cdot \hat{\zeta}_{\vec{r}}$  may not be the same. It is reasonable to assume that no specific choice will necessarily have the least numerical error, hence it is natural to use the average of the three candidates as the

average operation in Eq. (2.8). This technique is the one proposed in Ref. [12, 19]. Finally, Abe et al. [19] integrated metric identities into  $\frac{1}{3}(\vec{r}_{\xi^i} \cdot \hat{\xi}_{\vec{r}}^i)$  and obtained the conservative form  $\frac{1}{3}(\vec{r} \cdot \hat{\xi}_{\vec{r}}^i)_{\xi^i}$ .

Other than the above delicate considerations, revised Jacobian can be simply derived from some already-known basic formulae. In Ref. [9], the divergence of the vector  $\vec{A}$  in general coordinate system has the following definitions

$$\begin{cases} \nabla \cdot \vec{A} = (\sqrt{g} \cdot \vec{a}^i \cdot \vec{A}_{\xi^i}) / \sqrt{g}, \\ \nabla \cdot \vec{A} = (\sqrt{g} \cdot \vec{a}^i \cdot \vec{A})_{\xi^i} / \sqrt{g}, \end{cases} \quad (2.11)$$

where  $\vec{a}^i$  is the contravariant base vector defined as  $\sqrt{g} \cdot \vec{a}^i = \vec{r}_{\xi^j} \times \vec{r}_{\xi^k}$  with  $\sqrt{g} = \vec{r}_{\xi^i} \cdot (\vec{r}_{\xi^j} \times \vec{r}_{\xi^k})$ . Considering Eqs. (2.4) and (2.10), Eq. (2.11) becomes:  $\nabla \cdot \vec{A} = \frac{1}{J-1}(\hat{\xi}_{\vec{r}}^i \cdot \vec{A}_{\xi^i})$  or  $\nabla \cdot \vec{A} = \frac{1}{J-1}(\hat{\xi}_{\vec{r}}^i \cdot \vec{A})_{\xi^i}$ . Taking  $\vec{A}$  as  $\vec{r}$ , the following result is straightforward:

$$J^{-1} = \frac{1}{3}(\hat{\xi}_{\vec{r}}^i \cdot \vec{r}_{\xi^i}) \quad \text{or} \quad J^{-1} = \frac{1}{3}(\hat{\xi}_{\vec{r}}^i \cdot \vec{r})_{\xi^i}, \quad (2.12)$$

which is the same as that proposed by Abe et al. [19].

It is worth emphasizing again that although the numerical performance might possibly be improved by using Eq. (2.12) [12, 19], metric-caused errors should not theoretically arise from evaluation methods of Jacobian in stationary grids.

### 3 Approaches for linear upwind schemes with flux splitting to eliminate metric-caused errors

#### 3.1 More discussions on free-stream preservation

As mentioned in the introduction, some analysis on *FSP* [2] was based on Eq. (2.5) and started from Eq. (2.6). The acquisition of Eq. (2.6) relies on the presumption that constant fluxes can be moved outside of  $\delta$ . The process seems to be apparent at first look, but less distinct when flux splitting is imposed. More discussions are given next, and only linear difference scheme is used for simplicity.

Consider flux splitting at  $\xi$  direction as  $\hat{E} = \hat{E}^+ + \hat{E}^-$ . Suppose a  $r$ -th order scheme  $\delta_{\xi}^+$  for  $\hat{E}^+$  takes the form in Eq. (2.9) with  $m_1 \geq n_1$ , and  $m_1 + n_1 \geq r$ . It is obvious that the symmetric counterpart for  $\hat{E}^-$  will be

$$\delta_{\xi}^-(\cdot)_{i,j,k} = \frac{1}{\Delta} \sum_{i_1=-n_1}^{m_1} -a_{-i_1}^{\xi}(\cdot)_{i+i_1,j,k}.$$

If  $m_1 = n_1$  and  $a_{i_1}^{\tilde{\zeta}} = -a_{-i_1}^{\tilde{\zeta}}$ , the central scheme will be obtained with the denotation  $\delta_{\tilde{\zeta}}^c$ . It is trivial that

$$\delta_{\tilde{\zeta}}^c \hat{E}_{i,j,k}^+ + \delta_{\tilde{\zeta}}^c \hat{E}_{i,j,k}^- = \sum_{i_1=-m_1}^{m_1} a_{i_1}^{\tilde{\zeta}} \left( \hat{E}_{i+i_1,j,k}^+ + \hat{E}_{i+i_1,j,k}^- \right) = \sum_{i_1=-m_1}^{m_1} a_{i_1}^{\tilde{\zeta}} \hat{E}_{i+i_1,j,k} = \delta_{\tilde{\zeta}}^c \hat{E}_{i,j,k}. \quad (3.1)$$

So when the flow is uniform,

$$\begin{aligned} & \delta_{\tilde{\zeta}}^c (\hat{E}_{\infty}^+ + \hat{E}_{\infty}^-) + \delta_{\eta}^c (\hat{F}_{\infty}^+ + \hat{F}_{\infty}^-) + \delta_{\zeta}^c (\hat{G}_{\infty}^+ + \hat{G}_{\infty}^-) \\ &= \delta_{\tilde{\zeta}}^c (\hat{\zeta}_x E_{\infty} + \hat{\zeta}_y F_{\infty} + \hat{\zeta}_z G_{\infty}) + \dots \\ &= \left( \delta_{\tilde{\zeta}}^c \hat{\zeta}_x + \delta_{\eta}^c \hat{\eta}_x + \delta_{\zeta}^c \hat{\zeta}_x \right) E_{\infty} + \dots \\ &= E_{\infty} \cdot \vec{I}_x^* + F_{\infty} \cdot \vec{I}_y^* + G_{\infty} \cdot \vec{I}_z^*, \end{aligned}$$

where  $\vec{I}_{x_i}^* = \delta_{\tilde{\zeta}}^c \hat{\zeta}_{x_i} + \delta_{\eta}^c \hat{\eta}_{x_i} + \delta_{\zeta}^c \hat{\zeta}_{x_i}$  represents the numerical approximation of  $\vec{I}_{x_i}$  as before. Hence if a central scheme is used and  $MI$  could be attained, Eq. (2.6) can be established and  $FSP$  will be achieved.

For the upwind scheme,  $m_1 = n_1$  and  $a_{i_1}^{\tilde{\zeta}} = -a_{-i_1}^{\tilde{\zeta}}$  cannot be both satisfied. Therefore  $\delta_{\tilde{\zeta}}^+ \hat{E}^+ + \delta_{\tilde{\zeta}}^- \hat{E}^-$  cannot be re-arranged into a combination of worth to  $\hat{E}$  as in Eq. (3.1), and the constant fluxes would be difficult to be shifted out of the difference operator. Consequently Eq. (2.6) was thought to be hard to achieve by literatures [2, 9, 11], so was  $FSP$ . Therefore, a further investigation on linear *upwind* schemes with flux splitting to eliminate metric-caused errors will be meaningful and provide a foundation for further nonlinear implementations.

### 3.2 Approaches to eliminate metric-caused errors

In Ref. [23], a method to eliminate metric-caused errors is proposed for the fifth- and sixth-order nonlinear WENO schemes. In this section, a study from another perspective is introduced for generalized upwind schemes with the same purpose, which includes a proper decomposition and consideration on flux splitting. Then, a discussion is made regarding current study with that of Ref. [23].

(1) Central scheme decomposition (CSD) of upwind schemes.

Consider the  $r$ -th order upwind scheme  $\delta^+$  for the first-order derivative at position  $i$ , where indices like  $j, k$  are dropped for clarity. By Taylor expansion, there is

$$(\delta^+ f)_i = \partial f_i + a_{r+1} \partial^{(r+1)} f_i \times \Delta^r + a_{r+2} \partial^{(r+2)} f_i \times \Delta^{r+1} + \dots, \quad (3.2)$$

where  $a_i$  denotes the coefficient corresponding to the  $i$ -th order derivative.

Considering the symmetry, it is easy to find that for the counterpart  $\delta_i^-$ , when  $r$  is an even number, there will be

$$(\delta^- f)_i = \partial f_i + a_{r+1} \partial^{(r+1)} f_i \times \Delta^r - a_{r+2} \partial^{(r+2)} f_i \times \Delta^{r+1} + \dots, \quad (3.3)$$

while if  $r$  is an odd number,

$$(\delta^- f)_i = \partial f_i - a_{r+1} \partial^{(r+1)} f_i \times \Delta^r + a_{r+2} \partial^{(r+2)} f_i \times \Delta^{r+1} + \dots \quad (3.4)$$

The average of  $\delta^+$  and  $\delta^-$  can be uniformly expressed as

$$\begin{aligned} [(\delta^+ f)_i + (\delta^- f)_i] / 2 = & \partial f_i + a_{2[r/2]+1} \partial^{(2[r/2]+1)} f_i \times \Delta^{2[r/2]} \\ & + a_{2[r/2]+3} \partial^{(2[r/2]+3)} f_i \times \Delta^{2[r/2]+2} + \dots, \end{aligned} \quad (3.5)$$

which represents a central scheme with the accurate order  $2[r/2]$ .

Based on the above understanding, a central operator  $\delta^{c,(1)}$  is proposed as

$$(\delta^{c,(1)} f)_i = [(\delta^+ f)_i + (\delta^- f)_i] / 2, \quad (3.6)$$

where the number in superscript especially denotes the order of the derivative to approximate, namely,  $\partial f$ . Considering Eqs. (3.2) and (3.5),

$$\begin{aligned} (\delta^{c,(1)} f)_i - (\delta^+ f)_i = & -a_{2[r/2]+2} \partial^{(2[r/2]+2)} f_i \times \Delta^{2[r/2]+1} \\ & - a_{2[r/2]+4} \partial^{(2[r/2]+4)} f_i \times \Delta^{2[r/2]+3} + \dots, \end{aligned} \quad (3.7)$$

where only derivatives with even numbers exist on the right-hand side. Eq. (3.7) indicates its left-hand side regarding a central discretization of  $\partial^{(2[r/2]+2)} f_i$ . Define  $\delta^{c,(2[r/2]+2)}$  as

$$\delta^{c,(2[r/2]+2)} = (\delta^{c,(1)} f)_i - (\delta^+ f)_i. \quad (3.8)$$

It can be conceived that the expansion of Eq. (3.8) will have the form

$$\frac{1}{\Delta} \sum_{i_1=-m'}^{m'} a_{i_1}(\cdot)_{i+i_1}$$

with  $a_{i_1} = -a_{-i_1}$ ,  $m' = \max(m_1, n_1)$ , and

$$\sum_{i_1=-m'}^{m'} a_{i_1} = 0. \quad (3.9)$$

Similar analysis can be made toward  $\delta_i^-$ , and the following decompositions are obtained as

$$\begin{cases} (\delta^+ f)_i = (\delta^{c,(1)} f)_i - (\delta^{c,(2[r/2]+2)} f)_i, \\ (\delta^- f)_i = (\delta^{c,(1)} f)_i + (\delta^{c,(2[r/2]+2)} f)_i. \end{cases} \quad (3.10)$$

Because both  $\delta^{c,(1)}$  and  $\delta^{c,(2[r/2]+2)}$  are certain central schemes, the decomposition is referred as central scheme decomposition or CSD. In the next, CSD of three linear upwind schemes are presented as examples.

(a) CSD of the fifth-order upwind scheme.

The case represents an example of schemes with odd order numbers. For  $\delta^+$ :

$$(\delta^+ f)_i = \frac{1}{60\Delta} (-2f_{i-3} + 15f_{i-2} - 60f_{i-1} + 20f_i + 30f_{i+1} - 3f_{i+2}), \quad (3.11)$$

then,

$$(\delta^- f)_i = \frac{-1}{60\Delta} (-3f_{i-2} + 30f_{i-1} + 20f_i - 60f_{i+1} + 15f_{i+2} - 2f_{i+3}).$$

$\delta^{c,(1)}$ ,  $\delta^{c,(6)}$  and their Taylor expansions can be derived and shown in Table 1.

Table 1: CSD of the linear fifth-order upwind scheme and corresponding Taylor expansions.

Operator	Form	Taylor expansion
$\delta^{c,(1)}$	$\frac{1}{60\Delta} \begin{pmatrix} -f_{i-3} + 9f_{i-2} - 45f_{i-1} + \\ 45f_{i+1} - 9f_{i+2} + f_{i+3} \end{pmatrix}$	$f'_i + \frac{1}{140}f_i^{(7)}\Delta^6 + \frac{1}{720}f_i^{(9)}\Delta^8 + \dots$
$\delta^{c,(6)}$	$\frac{1}{60\Delta} \begin{pmatrix} f_{i-3} - 6f_{i-2} + 15f_{i-1} - 20f_i + \\ 15f_{i+1} - 6f_{i+2} + f_{i+3} \end{pmatrix}$	$\frac{1}{60}f_i^{(6)}\Delta^5 + \frac{1}{240}f_i^{(8)}\Delta^7 + \dots$

(b) CSD of the second-order upwind scheme.

The case shows an example of schemes with even order numbers. The form of  $\delta^+$  is:

$$(\delta^+ f)_i = \frac{1}{2\Delta} (f_{i-2} - 4f_{i-1} + 3f_i). \quad (3.12)$$

Similarly,  $\delta^{c,(1)}$  and  $\delta^{c,(4)}$  together with their Taylor expansions can be summarized in Table 2. It is worth mentioning that  $\delta^{c,(1)}$  is a second-order discretization and not of the optimal fourth-order at the dependent stencil.

Table 2: CSD of the linear second-order upwind scheme and corresponding Taylor expansions.

Operator	Form	Taylor expansion
$\delta^{c,(1)}$	$\frac{1}{4\Delta} (f_{i-2} - 4f_{i-1} + 4f_{i+1} - f_{i+2})$	$f'_i - \frac{1}{3}f_i^{(3)}\Delta^2 - \frac{7}{60}f_i^{(5)}\Delta^4 + \dots$
$\delta^{c,(4)}$	$\frac{1}{4\Delta} (-f_{i-2} + 4f_{i-1} - 6f_i + 4f_{i+1} - f_{i+2})$	$-\frac{1}{4}f_i^{(4)}\Delta^3 - \frac{1}{24}f_i^{(6)}\Delta^5 + \dots$

(c) CSD of a third-order mixed node/half-node-type scheme.

In Ref. [20], Zhang proposed a method to derive the high-order conservative schemes. Following the idea, we recently derived series of high-order mixed node/half-node-type schemes. The linear form of the third-order case is:

$$(\delta^+ f)_i = \frac{1}{\Delta} \times \left[ \frac{1}{3}(f_i - f_{i-1}) + \frac{1}{6}(5f_{i+1/2} - 6f_{i-1/2} + f_{i-3/2}) \right]. \quad (3.13)$$

Table 3: CSD of the linear third-order upwind scheme and corresponding Taylor expansions.

Operator	Form		Taylor expansion
$\delta^{c,(1)}$	$\frac{1}{12\Delta}$	$2(f_{i+1}-f_{i-1})+(-f_{i+3/2}+11f_{i+1/2}-11f_{i-1/2}+f_{i-3/2})$	$f'_i - \frac{7}{960}f_i^{(5)}\Delta^4 - \frac{f_i^{(7)}\Delta^6}{2016} + \dots$
$\delta^{c,(4)}$	$\frac{1}{12\Delta}$	$2(f_{i+1}-2f_i+f_{i-1})+(-f_{i+3/2}+f_{i+1/2}+f_{i-1/2}-f_{i-3/2})$	$-\frac{1}{48}f_i^{(4)}\Delta^3 - \frac{5}{2304}f_i^{(6)}\Delta^5 + \dots$

Similarly,  $\delta^{c,(1)}$ ,  $\delta^{c,(4)}$  and their Taylor expansions are summarized in Table 3.

In short, through CSD, arbitrary upwind schemes can be decomposed into two central schemes.

(2) Analysis on flux splitting to achieve free-stream preservation.

Because  $\delta^+$  and  $\delta^-$  act on different split fluxes, i.e.,  $\delta^+\hat{E}^+ + \delta^-\hat{E}^-$ , it seems that only  $\delta^{c,(1)}$  in Eq. (3.10) satisfies *FSP* according to Section 3.1, while the operation of  $\delta^{c,(2\lfloor r/2 \rfloor + 2)}$  on  $\hat{E}^+$  and  $\hat{E}^-$  might not generally cancel out each other. Next, it will be shown that the cancellation can be achieved by Eq. (3.10) under free-stream condition if the following requirement for flux splitting is followed.

Consider a flux splitting scheme as

$$\hat{E}^\pm = \frac{1}{2}(\hat{E} \pm \hat{A} \cdot Q) \quad \text{or} \quad \hat{E}^\pm = \frac{1}{2}(\hat{E} \pm \hat{E}_{ref}), \quad (3.14)$$

where  $\hat{A}$  denotes certain constant matrix or number and  $\hat{E}_{ref}$  represents some referenced flux. The following requirement is proposed for  $\hat{A}$  and  $\hat{E}_{ref}$  in order to achieve *FSP*: when the uniform-flow condition is imposed,  $\hat{A}$  and  $\hat{E}_{ref}$  are supposed to be locally constant at least at the dependent stencil of  $\delta^{c,(2\lfloor r/2 \rfloor + 2)}$ . Then considering Eqs. (3.9) and (3.14), the part regarding  $\delta^{c,(2\lfloor r/2 \rfloor + 2)}$  in  $\delta^+\hat{E}^+ + \delta^-\hat{E}^-$  by Eq. (3.10) will become

$$\begin{aligned} & \delta^{c,(2\lfloor r/2 \rfloor + 2)}(\hat{E}_\infty^+) - \delta^{c,(2\lfloor r/2 \rfloor + 2)}(\hat{E}_\infty^-) \\ &= \begin{cases} \frac{1}{2} \sum_{i_1=-m'}^{m'} a_{i_1} (\hat{E}_{i+i_1} - \hat{E}_{i+i_1})_\infty + \frac{\hat{A}Q_\infty}{\Delta} \sum_{i_1=-m'}^{m'} a_{i_1} = 0 & \text{or} \\ \frac{1}{2} \sum_{i_1=-m'}^{m'} a_{i_1} (\hat{E}_{i+i_1} - \hat{E}_{i+i_1})_\infty + \frac{\hat{E}_{ref}}{\Delta} \sum_{i_1=-m'}^{m'} a_{i_1} = 0. \end{cases} \end{aligned} \quad (3.15)$$

Therefore, under the uniform flow, the contribution of  $\delta^{c,(2\lfloor r/2 \rfloor + 2)}$  in  $\delta^+\hat{E}_\infty^+ + \delta^-\hat{E}_\infty^-$  will be null, and only the action of  $\delta^{c,(1)}$  will be left which is also zero. Hence *FSP* is acquired for arbitrary upwind schemes through CSD.

In the following, a Lax-Friedrichs-type scheme is given as an example through realizing a concrete  $\hat{A}$  in Eq. (3.14). First consider a referenced splitting

$$\hat{E}^\pm = \frac{1}{2}(\hat{E} \pm \Lambda \cdot Q), \quad (3.16)$$

where  $\Lambda = \text{diag}(\lambda_1, \dots, \lambda_5) = \text{diag}(\hat{U}, \hat{U}, \hat{U}, \hat{U} - c|\hat{\xi}|, \hat{U} + c|\hat{\xi}|)$ ,  $\hat{U} = \hat{\xi}_{x_j} w_j$ ,  $c$  is the sound speed and  $|\hat{\xi}| = (\hat{\xi}_{x_j} \cdot \hat{\xi}_{x_j})^{1/2}$ . In order to achieve aforementioned requirement,  $\Lambda$  in Eq. (3.16) is revised to compose  $\hat{A}$  by:  $\hat{A} = \text{MAX}(\max_{k=1, \dots, 5} |\lambda_k|) \cdot I$  or  $\hat{A} = \text{diag}(\text{MAX}|\lambda_1|, \dots, \text{MAX}|\lambda_5|)$ , where  $I$  is the identity matrix and the maximum operator  $\text{MAX}$  should run over the whole field or the dependent stencil of  $\delta^{c(1)}$  from  $i - m'$  to  $i + m'$ . From previous discussions, it can be seen that Eq. (3.15) will be established thereafter. In this study, the former form of  $\hat{A}$  and the whole field are chosen for tests. It can be conceived similar treatment can be adopted for splitting like Steger - Warming method. Thus far, if  $\delta^{c(1)}$  by CSD is used for metric approximation and above flux splitting is adopted,  $FSP$  can be achieved for arbitrary linear upwind schemes by  $\delta^+ \hat{E}^+ + \delta^- \hat{E}^-$ .

(3) Discussions about current study with that in Ref. [23].

In Ref. [23], the original fifth- and sixth-order WENO schemes were transformed into one consistent central part plus two nonlinear dissipation parts respectively. Considering the fifth-order WENO in the reference, the one for  $h_{i+1/2}$  in  $\left(\frac{\partial \hat{E}}{\partial \xi}\right)_i = \frac{h_{i+1/2} - h_{i-1/2}}{\Delta \xi}$  was revised as [23]:

$$\begin{aligned} h_{j+1/2} = & \frac{1}{60} (\hat{E}_{i-2} - 8\hat{E}_{i-1} + 37\hat{E}_i + 37\hat{E}_{i+1} - 8\hat{E}_{i+2} + \hat{E}_{i+3}) \\ & - \frac{1}{60} \left\{ (20\omega^{+,1} - 1) \hat{\varepsilon}_{i-2}^+ - [10(\omega^{+,1} + \omega^{+,2}) - 5] \hat{\varepsilon}_{i-1}^+ + \hat{\varepsilon}_i^+ \right\} \\ & + \frac{1}{60} \left\{ (20\omega^{-,1} - 1) \hat{\varepsilon}_i^- - [10(\omega^{-,1} + \omega^{-,2}) - 5] \hat{\varepsilon}_{i-1}^- + \hat{\varepsilon}_{i-2}^- \right\}, \end{aligned} \quad (3.17)$$

where  $\hat{\varepsilon}_k^\pm = (-\hat{E}_k^\pm + 3\hat{E}_{k+1}^\pm - 3\hat{E}_{k+2}^\pm + \hat{E}_{k+3}^\pm)$ , and  $\{\omega^{+,1}, \omega^{+,2}, \omega^{-,1}, \omega^{-,2}\}$  are canonical nonlinear weights of WENO corresponding to their linear counterparts  $\{0.1, 0.6, 0.1, 0.6\}$  respectively [22]. To acquire  $FSP$ , a flux splitting by freezing metrics at  $i+1/2$  was proposed as:

$$\hat{E}_{i+i_1}^\pm = (\hat{\xi}_x, \hat{\xi}_y, \hat{\xi}_z)_{i+1/2} \cdot (E, F, G)_{i+i_1}^T \pm \Lambda_{i+1/2} \cdot J_{i+1/2}^{-1} Q. \quad (3.18)$$

In addition, the derivatives of coordinates such as  $x_{\hat{\xi}}$  use the similar conservative scheme as  $\frac{\partial \hat{E}}{\partial \xi}$ , where only the central part in Eq. (3.17) is used in  $h_{i+1/2}$ .

If  $\delta^{c(1)}$  in Table 1 is expressed in conservative form, it is easy to test that  $h_{i+1/2}$  will be the same as the central part in Eq. (3.17). Therefore, the linear counterpart of Eq. (3.17), which can be simply derived by replacing nonlinear weights with the linear correspondence, is consistent with Eq. (3.11). However, Eq. (3.11) does not explicitly use a central scheme like that in Eq. (3.17), and practical performances of two methods show differences in vortex-preservation computation in Section 5. Moreover, when M-UPW3 by Eq. (3.13) is extended to its nonlinear version, its conservative form will be shown as  $h_{i+1/2}^+ = \frac{1}{3} \hat{E}_i^+ + \frac{1}{6} (5\hat{E}_{i+1/2}^+ - \hat{E}_{i-1/2}^+)$ , and the nonlinearity is planned to be introduced by nonlinear interpolations at half nodes as that in Ref. [22]. Once again in this occasion, no central scheme will be explicitly used for flux derivatives, and the nonlinear implementation will be substantially different from that in Ref. [23].

Another difference of current study with Ref. [23] lies in the treatment of flux splitting. It is easy to see from Eq. (3.18) that  $\hat{E}_{i+i_1} \neq \hat{E}_{i+i_1}^+ + \hat{E}_{i+i_1}^-$ , and the frozen disposal of metrics is suspected to introduce errors theoretically. In turn, current method with the form as Eq. (3.14) is free of such problem.

## 4 Directionally consistent interpolation for half-node or mixed-type schemes

### 4.1 Analysis on derivation for variables at half nodes and directionally consistent interpolation

It is conceivable that algorithms to eliminate errors in metric evaluation in previous sections straightforwardly work for node-type linear difference schemes. While for half-node- or mixed-type schemes, in order to evaluate the flux  $\hat{E}^\pm$  at half nodes, metrics at the cell edges should be prepared first. Their acquisition usually employs the following way: first, evaluate the metrics at nodes firstly, then interpolate them to the half nodes [11]. In Ref. [11], the sixth- or fourth-order interpolation was suggested as a candidate. In order to derive the metrics at nodes, coordinates and their derivatives at half nodes are still needed for half-node- or mixed-type schemes. In this regard, the derivatives are suggested to be computed by  $\delta^{c,(1)}$  according to Section 3, while coordinates at half nodes are acquired again by interpolations. For example, if  $\delta^+$  by Eq. (3.13) and its counterpart  $\delta^-$  are used to discretize  $\partial_{\xi}(\hat{E}^\pm)_{i,j,k}$ , grid metrics like  $(\hat{\xi}_x)_{i+i_1+1/2,j,k}$  should be evaluated by using Eq. (2.7) or (2.8). In order to derive grid metrics like  $(\hat{\xi}_x)_{i+i_1+1/2,j,k'}$  series of  $(\hat{\xi}_x)_{i+i_1+i_2,j,k}$  are first computed by using the same  $\delta^{c,(1)}$ . Next, the interpolation like the fourth-order scheme in Table 4 is used to derive  $\hat{\xi}_x$  at  $(i+i_1+1/2,j,k)$ . For derivatives like  $y_\eta$  in  $(\hat{\xi}_x)_{i+i_1+i_2,j,k'}$  they are again evaluated by  $\delta^{c,(1)}$ , where coordinates needed at half nodes are similarly interpolated from coordinates at nodes.

From the above discussion, it can be seen that the use of interpolations is not fully ascertained, and the relationship between interpolations and *MI* was not seriously studied in past literatures. It will be shown in Section 4.2 that for half-node- or mixed-type schemes, even if techniques like consistent schemes and Eq. (2.7) or (2.8) are employed, *MI* could still be violated if interpolations are not treated properly. To deal with this problem, an idea of directionally consistent interpolation, namely *DCI*, is proposed: the consistent linear interpolation should be imposed on each coordinate direction in the evaluation of metrics and fluxes, while the interpolations could be different in different directions. Analysis will be given in the following.

First, preliminary analysis is made to show that if the variables at half nodes are theoretically available and unique, numerical commutativity of the mixed derivative  $\partial_{\xi\zeta}$  can be attained by using mixed-type linear schemes. Similar to Eq. (2.9), general forms of

the schemes are supposed to be:

$$\begin{cases} \delta_{\zeta}^{\zeta}(\cdot)_{i,j,k} = \sum_{i_1=-m_1}^{n_1} a_{i_1}^{\zeta}(\cdot)_{i+i_1,j,k} + \sum_{i_2=-m_2}^{n_2} b_{i_2}^{\zeta}(\cdot)_{i+i_2+1/2,j,k'} \\ \delta_{\zeta}^{\zeta}(\cdot)_{i,j,k} = \sum_{k_1=-m_3}^{n_3} a_{k_1}^{\zeta}(\cdot)_{i,j,k+k_1} + \sum_{k_2=-m_4}^{n_4} b_{k_2}^{\zeta}(\cdot)_{i,j,k+k_2+1/2'} \end{cases} \quad (4.1)$$

where  $a_{i_1}^{\zeta}, b_{i_2}^{\zeta}, a_{k_1}^{\zeta}$  and  $b_{k_2}^{\zeta}$  denote coefficients of schemes. Then for any function  $f_{i,j,k}$ ,

$$\begin{aligned} \delta_{\zeta}^{\zeta} \delta_{\zeta}^{\zeta}(f)_{i,j,k} &= \sum_{i_1=-m_1}^{n_1} \sum_{k_1=-m_3}^{n_3} a_{i_1}^{\zeta} a_{k_1}^{\zeta} f_{i+i_1,j,k+k_1} + \sum_{i_1=-m_1}^{n_1} \sum_{k_2=-m_4}^{n_4} a_{i_1}^{\zeta} b_{k_2}^{\zeta} f_{i+i_1,j,k+k_2+1/2} \\ &+ \sum_{i_2=-m_2}^{n_2} \sum_{k_1=-m_3}^{n_3} b_{i_2}^{\zeta} a_{k_1}^{\zeta} f_{i+i_2+1/2,j,k+k_1} + \sum_{i_2=-m_2}^{n_2} \sum_{k_2=-m_4}^{n_4} b_{i_2}^{\zeta} b_{k_2}^{\zeta} f_{i+i_2+1/2,j,k+k_2+1/2} \end{aligned} \quad (4.2)$$

and

$$\begin{aligned} \delta_{\zeta}^{\zeta} \delta_{\zeta}^{\zeta}(f)_{i,j,k} &= \sum_{k_1=-m_3}^{n_3} \sum_{i_1=-m_1}^{n_1} a_{k_1}^{\zeta} a_{i_1}^{\zeta} f_{i+i_1,j,k+k_1} + \sum_{k_2=-m_4}^{n_4} \sum_{i_1=-m_1}^{n_1} b_{k_2}^{\zeta} a_{i_1}^{\zeta} f_{i+i_1,j,k+k_2+1/2} \\ &+ \sum_{k_1=-m_3}^{n_3} \sum_{i_2=-m_2}^{n_2} a_{k_1}^{\zeta} b_{i_2}^{\zeta} f_{i+i_2+1/2,j,k+k_1} + \sum_{k_2=-m_4}^{n_4} \sum_{i_2=-m_2}^{n_2} b_{k_2}^{\zeta} b_{i_2}^{\zeta} f_{i+i_2+1/2,j,k+k_2+1/2}. \end{aligned} \quad (4.3)$$

It is clear that  $\delta_{\zeta}^{\zeta} \delta_{\zeta}^{\zeta}(f)_{i,j,k} = \delta_{\zeta}^{\zeta} \delta_{\zeta}^{\zeta}(f)_{i,j,k}$  providing variables at half nodes are consistent at the same position in two equations.

Next, interpolations to derive variables at half nodes are discussed. As discussed before, Eqs. (4.2)-(4.3) play a key role in metric cancellation if Eq. (2.7) or (2.8) is used for metric derivation. It is worth recalling that the outer derivative  $\partial_{\zeta}^j$  in  $I_{x_i} \equiv (\hat{\zeta}_{x_i}^j)_{\zeta_j}$  by Eq. (2.3) actually originates from the operator on fluxes in Eq. (2.2), while derivatives inside  $\hat{\zeta}_{x_i}^j$  come from grid metrics. Based on above understanding, taking  $\delta_{\zeta}^{\zeta} \delta_{\zeta}^{\zeta}$  in Eq. (4.2) for illustration,  $\delta_{\zeta}^{\zeta}$  in  $\delta_{\zeta}^{\zeta} \delta_{\zeta}^{\zeta}$  is supposed to relate to flux derivative, while  $\delta_{\zeta}^{\zeta}$  should correspond the outer derivative in grid metrics like  $\partial_{\zeta}^k$  in  $[(x_j)_{\zeta_j} \cdot x_{k'}]_{\zeta_k}$  in Eq. (2.7). When Eq. (4.1) is used to discretize flux derivative and grid metrics, interpolations will be triggered. Let the interpolation in  $\zeta$  direction for flux derivative denoted as  $X_{\zeta}^F$  and the one for grid metrics represented by  $X_{\zeta}^G$ , and let interpolations have the general forms

$$\begin{cases} X_{\zeta}^F(\cdot)_{i,j,k+1/2} = \sum_{k_3=-m_F}^{n_F} c_{k_3}^F(\cdot)_{i,j,k+k_3'} \\ X_{\zeta}^G(\cdot)_{i,j,k+1/2} = \sum_{k_3=-m_G}^{n_G} c_{k_3}^G(\cdot)_{i,j,k+k_3'} \end{cases} \quad (4.4)$$

where  $c_{k_3}^F$  and  $c_{k_3}^G$  denote coefficients of interpolations, and where scripts "F" and "G" denotes operations on flux and grid metric respectively. Taking the second terms in Eq. (4.2) and (4.3) for illustration, if  $f$  at half nodes are interpolated by Eq. (4.4), then the second term in Eq. (4.2) becomes

$$\sum_{k_2=-m_4}^{n_4} \sum_{i_1=-m_1}^{n_1} b_{k_2}^{\zeta} a_{i_1}^{\xi} X_{\zeta}^G(f)_{i+i_1, j, k+k_2+1/2} = \sum_{k_2=-m_4}^{n_4} \sum_{i_1=-m_1}^{n_1} \sum_{k_3=-m_G}^{n_G} b_{k_2}^{\zeta} a_{i_1}^{\xi} c_{k_3}^G(f)_{i+i_1, j, k+k_2+k_3}$$

and the second term in Eq. (4.3) becomes

$$\sum_{k_2=-m_4}^{n_4} \sum_{i_1=-m_1}^{n_1} b_{k_2}^{\zeta} a_{i_1}^{\xi} X_{\zeta}^F(f)_{i+i_1, j, k+k_2+1/2} = \sum_{k_2=-m_4}^{n_4} \sum_{i_1=-m_1}^{n_1} \sum_{k_3=-m_F}^{n_F} b_{k_2}^{\zeta} a_{i_1}^{\xi} c_{k_3}^F(f)_{i+i_1, j, k+k_2+k_3}.$$

Comparing the above two terms, it is obvious that if  $m_F = m_G$ ,  $n_F = n_G$  and  $c_{k_3}^F = c_{k_3}^G$ , they will become the same. Similarly, the third and fourth terms in Eqs. (4.3)-(4.4) will be equal under the same assumption, therefore  $\delta_{\zeta} \delta_{\xi}(f)_{i, j, k} = \delta_{\xi} \delta_{\zeta}(f)_{i, j, k}$ . Hence, with the employment of  $X_{\zeta^i}^F = X_{\zeta^i}^G$  or *DCI*, numerical commutativity of all mixed derivatives is acquired and therefore  $I_{\vec{r}} = 0$  is established.

Finally, it is worth mentioning that in Eq. (2.7) or (2.8), there are still derivative terms inside the outer derivative, e.g.,  $(x_{j'})_{\zeta^j}$  in  $[(x_{j'})_{\zeta^j} \cdot x_{k'}]_{\zeta^k}$ . Their evaluations at nodal points will still need to use coordinates at half nodes derived by interpolations (denoted as  $X_{\zeta^i}^{G, in}$ ). Theoretically,  $X_{\zeta^i}^{G, in}$  does not need to be the same as  $X_{\zeta^i}^G$ , and it can be found that the consistent use of  $X_{\zeta^i}^{G, in}$  in each  $\zeta^i$  will yield *MI* under  $X_{\zeta^i}^F = X_{\zeta^i}^G$ . Subsequent numerical test validates this implementation. However, the choice of  $X_{\zeta^i}^G = X_{\zeta^i}^{G, in}$  will be more convenient in coding and therefore be preferred by applications. What is more, our practices indicated more numerical oscillations were observed when  $X_{\zeta^i}^G \neq X_{\zeta^i}^{G, in}$  was used.

## 4.2 Numerical validations

To validate the analysis in the previous section, five cases are designed to evaluate  $\vec{I}_{\vec{r}}$  on a 3-D randomized grid in Section 5.1 with the dimension  $41^3$ . In the computation, Eq. (2.8) is chosen to formulate  $\hat{\zeta}_{\vec{r}}^i$  first, then the CSD of M-UPW3 or  $\delta^{c, (1)}$  in Table 3 is used for discretization; after  $\hat{\zeta}_{\vec{r}}^i$  is evaluated,  $\vec{I}_{\vec{r}}$  will be computed by the same  $\delta^{c, (1)}$  again. During the process, variables at half nodes are interpolated repeatedly as discussed above. For comparative study, three interpolations are chosen with orders from fourth to sixth [21, 22] and are shown in Table 4.

To illustrate the effect of interpolations, five cases are carefully designed to show the validity and necessity of *DCI*. The details of interpolations in cases are as follows:

(1) Case I: In evaluations of  $\hat{\zeta}_{\vec{r}}^i$  and  $\vec{I}_{\vec{r}}$ , the fourth-order interpolation is uniformly used for  $X_{\zeta^i}^G$ ,  $X_{\zeta^i}^{G, in}$  and  $X_{\zeta^i}^F$  in three curvilinear coordinate directions.

Table 4: Forms of fourth-, fifth- and sixth-order interpolations.

Order	Forms of interpolations
4	$f_{i+1/2} \approx \frac{1}{16}(-f_{i-1} + 9f_i + 9f_{i+1} - f_{i+2})$
5	$f_{i+1/2} \approx \frac{1}{128}(3f_{i-2} - 20f_{i-1} + 90f_i + 60f_{i+1} - 5f_{i+2})$
6	$f_{i+1/2} \approx \frac{1}{256}(3f_{i-2} - 25f_{i-1} + 150f_i + 150f_{i+1} - 25f_{i+2} + 3f_{i+3})$

(2) Case II: In the evaluation of  $\hat{\zeta}_{\vec{r}}^i$ , the same fourth-order interpolations for  $X_{\zeta^i}^G$  and  $X_{\zeta^i}^{G,in}$  are chosen as in Case I. In the computation of  $\vec{I}_{\vec{r}}$  afterwards, the sixth-order interpolation for  $X_{\zeta^i}^F$  is used for  $\eta$  direction and the same fourth-order one is used for the rest directions, which indicates a violation of DCI.

(3) Case III: In the evaluation of  $\hat{\zeta}_{\vec{r}}^i$ , the fourth-order interpolation for  $X_{\zeta^i}^G$  and  $X_{\zeta^i}^{G,in}$  is used in  $\zeta$  direction, the fifth-order one is used in  $\eta$  direction, and the sixth-order one is used in  $\xi$  direction. Afterwards, the same choices of interpolation for  $X_{\zeta^i}^F$  are used to evaluate  $\vec{I}_{\vec{r}}$ .

(4) Case IV: Interpolations are the same as those in Case III except that in the computation of  $\vec{I}_{\vec{r}}$ , the sixth-order interpolation is used for  $X_{\zeta^i}^F$  in  $\zeta$  direction, which indicates a violation of DCI.

(5) Case V: Interpolations are the same as those in Case III except that in the evaluation of  $\hat{\zeta}_{\vec{r}}^i$ , the sixth-order interpolation is used for  $X_{\zeta^i}^{G,in}$  in  $\zeta$  direction.

The use of interpolations and their coincidence with DCI are summarized in Table 5.

Table 5: Tests of interpolations in the evaluation of metric identities by using M-UPW3.

	Orders of interpolations $X_{\zeta^i}^{G,in} / X_{\zeta^i}^G / X_{\zeta^i}^F$ in different directions			
	$\xi$	$\eta$	$\zeta$	DCI
case I	4/4/4	4/4/4	4/4/4	√
case II	4/4/4	4/4/6	4/4/4	×
case III	4/4/4	5/5/5	6/6/6	√
case IV	4/4/6	5/5/5	6/6/6	×
case V	6/4/4	5/5/5	6/6/6	√

Values of  $\vec{I}_{\vec{r}}$  in five cases are computed and shown in Table 6, where

$$\|\cdot\| = \sqrt{\frac{\sum_{i=1}^N (\cdot)_i^2}{N}}$$

and  $N$  is the total grid number.

Table 6: Values of  $\vec{I}_f$  in five cases of implementations of interpolations.

Cases	$  I_x  $	$  I_y  $	$  I_z  $
case I	5.875271E-012	5.846736E-012	5.786077E-012
case II	23.911432	33.977481	24.252242
case III	6.25142E-012	6.373999E-012	6.570719E-012
case IV	40.855302	29.04189	28.667106
case V	9.04020E-012	9.37979E-012	9.50324E-012

From the table, it is obvious that  $MI$  is preserved in case I, III and V, while violations occur in case II and IV even if Eq. (2.8) and the consistent M-UPW3 are used. Hence, the computation validates the analysis in Section 4.2.

### 4.3 Short summary on numerical implementations

Based on the above analysis, a summary is made on numerical implementations:

(1) Given any linear upwind scheme  $\delta^+$  (and  $\delta^-$  accordingly),  $\delta^{c,(1)}$  is derived by Eq. (3.6).

*For evaluations of grid metrics and Jacobian*

(2) Eq. (2.7) or (2.8) is chosen as the derivation form of grid metrics, while  $\delta^{c,(1)}$  is used for evaluations. Eq. (2.8) is used in this study.

To facilitate coding, the expanded forms of  $\hat{\xi}_f^i$  by Eq. (2.7) are given as

$$\begin{aligned}\hat{\xi}_x &= (y_\eta \cdot z)_\zeta - (y_\zeta \cdot z)_\eta, & \hat{\xi}_y &= (z_\eta \cdot x)_\zeta - (z_\zeta \cdot x)_\eta, & \hat{\xi}_z &= (x_\eta \cdot y)_\zeta - (x_\zeta \cdot y)_\eta, \\ \hat{\eta}_x &= (y_\zeta \cdot z)_\xi - (y_\xi \cdot z)_\zeta, & \hat{\eta}_y &= (z_\zeta \cdot x)_\xi - (z_\xi \cdot x)_\zeta, & \hat{\eta}_z &= (x_\zeta \cdot y)_\xi - (x_\xi \cdot y)_\zeta, \\ \hat{\zeta}_x &= (y_\xi \cdot z)_\eta - (y_\eta \cdot z)_\xi, & \hat{\zeta}_y &= (z_\xi \cdot x)_\eta - (z_\eta \cdot x)_\xi, & \hat{\zeta}_z &= (x_\xi \cdot y)_\eta - (x_\eta \cdot y)_\xi.\end{aligned}$$

and the forms by Eq. (2.8) are

$$\begin{aligned}\hat{\xi}_x &= \frac{1}{2} \begin{bmatrix} (y_\eta \cdot z)_\zeta - (y_\zeta \cdot z)_\eta \\ + (z_\zeta \cdot y)_\eta - (z_\eta \cdot y)_\zeta \end{bmatrix}, & \hat{\xi}_y &= \frac{1}{2} \begin{bmatrix} (z_\eta \cdot x)_\zeta - (z_\zeta \cdot x)_\eta \\ + (x_\zeta \cdot z)_\eta - (x_\eta \cdot z)_\zeta \end{bmatrix}, & \hat{\xi}_z &= \frac{1}{2} \begin{bmatrix} (x_\eta \cdot y)_\zeta - (x_\zeta \cdot y)_\eta \\ + (y_\zeta \cdot x)_\eta - (y_\eta \cdot x)_\zeta \end{bmatrix}, \\ \hat{\eta}_x &= \frac{1}{2} \begin{bmatrix} (y_\zeta \cdot z)_\xi - (y_\xi \cdot z)_\zeta \\ + (z_\xi \cdot y)_\zeta - (z_\zeta \cdot y)_\xi \end{bmatrix}, & \hat{\eta}_y &= \frac{1}{2} \begin{bmatrix} (z_\zeta \cdot x)_\xi - (z_\xi \cdot x)_\zeta \\ + (x_\xi \cdot z)_\zeta - (x_\zeta \cdot z)_\xi \end{bmatrix}, & \hat{\eta}_z &= \frac{1}{2} \begin{bmatrix} (x_\zeta \cdot y)_\xi - (x_\xi \cdot y)_\zeta \\ + (y_\xi \cdot x)_\zeta - (y_\zeta \cdot x)_\xi \end{bmatrix}, \\ \hat{\zeta}_x &= \frac{1}{2} \begin{bmatrix} (y_\xi \cdot z)_\eta - (y_\eta \cdot z)_\xi \\ + (z_\eta \cdot y)_\xi - (z_\xi \cdot y)_\eta \end{bmatrix}, & \hat{\zeta}_y &= \frac{1}{2} \begin{bmatrix} (z_\xi \cdot x)_\eta - (z_\eta \cdot x)_\xi \\ + (x_\eta \cdot z)_\xi - (x_\xi \cdot z)_\eta \end{bmatrix}, & \hat{\zeta}_z &= \frac{1}{2} \begin{bmatrix} (x_\xi \cdot y)_\eta - (x_\eta \cdot y)_\xi \\ + (y_\eta \cdot x)_\xi - (y_\xi \cdot x)_\eta \end{bmatrix}.\end{aligned}$$

The evaluation of grid metrics are undertaken by replacing the partial differential operator with the corresponding difference one. Taking the evaluation of  $(y_\eta \cdot z)_\zeta$  in  $\hat{\xi}_x$

at nodes for example, first  $y_\eta$  is evaluated at nodes by  $\delta^{c,(1)}(y)$  along  $\eta$ -direction, then  $(y_\eta \cdot z)_\zeta$  is evaluated by  $\delta^{c,(1)}((y_\eta)^* \cdot z)$  along  $\zeta$ -direction, where  $(y_\eta)^*$  denotes the numerical approximation of  $y_\eta$  obtained just now.

(3) Eq. (2.12) is suggested for the derivation of Jacobian, and the second form in the equation is chosen in this study. Especially,  $\hat{\xi}_r^i$  in the equation should be evaluated by step (2). To avoid misapprehension, it is worth repeating that the conservative form of Jacobian does not contribute to the elimination of metric-caused errors theoretically in stationary grids.

Still in order to facilitate coding, the expanded forms of  $J^{-1}$  by Eq. (2.12) are given as

$$J^{-1} = \frac{1}{3} \begin{bmatrix} \hat{\xi}_x \cdot x_\zeta + \hat{\xi}_y \cdot y_\zeta + \hat{\xi}_z \cdot z_\zeta \\ + \hat{\eta}_x \cdot x_\eta + \hat{\eta}_y \cdot y_\eta + \hat{\eta}_z \cdot z_\eta \\ + \hat{\xi}_x \cdot x_\zeta + \hat{\xi}_y \cdot y_\zeta + \hat{\xi}_z \cdot z_\zeta \end{bmatrix} \quad \text{or} \quad J^{-1} = \frac{1}{3} \begin{bmatrix} (\hat{\xi}_x \cdot x)_\zeta + (\hat{\xi}_y \cdot y)_\zeta + (\hat{\xi}_z \cdot z)_\zeta \\ + (\hat{\eta}_x \cdot x)_\eta + (\hat{\eta}_y \cdot y)_\eta + (\hat{\eta}_z \cdot z)_\eta \\ + (\hat{\xi}_x \cdot x)_\zeta + (\hat{\xi}_y \cdot y)_\zeta + (\hat{\xi}_z \cdot z)_\zeta \end{bmatrix}$$

and their numerical evaluations can be obtained similarly.

*For evaluations of flux derivatives*

(4) Flux splitting method described in Section 3.2 should be used, and the derivatives of the split flux are discretized by the given  $\delta^+$  and  $\delta^-$ .

*For half-node- or mixed-type schemes, interpolations must be used in the above steps to derive variables and grid metrics at half nodes, and*

(5) DCI should be followed to achieve MI and elimination of metric-caused errors.

The above procedures are valid for central schemes as well except that the restriction for flux splitting can be released, e.g., the fourth-order central scheme can be used for both the flux and metric evaluation.

## 5 Numerical validations

In this section, two canonical problems, one regarding *FSP* and the other about the isentropic vortex preservation, are tested by using 2-D Euler equations. The problems are favored by studies on metric-evoked errors. Two upwind schemes for spatial discretizations are used, namely, the fifth-order upwind scheme by Eq. (3.11) (UPW5) and the third-order mixed upwind scheme by Eq. (3.13) (M-UPW3). To combine with M-UPW3, the fourth-order interpolation in Table 5 is used to derive variables at half nodes. For reference, the fourth-order central scheme (CS4) is also realized. To enhance its numerical stability in some computations, a sixth-order compact filter (CF6) [21] is used as:

$$\alpha_f \bar{f}_{i-1} + \bar{f}_i + \alpha_f \bar{f}_{i+1} = \frac{1}{2} \left[ \begin{aligned} & \left( \frac{11}{16} + \frac{5\alpha_f}{8} \right) f_i + \left( \frac{15}{32} + \frac{17\alpha_f}{16} \right) (f_{i+1} + f_{i-1}) + \\ & \left( \frac{-3}{16} + \frac{3\alpha_f}{8} \right) (f_{i+2} + f_{i-2}) + \left( \frac{1}{32} - \frac{\alpha_f}{16} \right) (f_{i+3} + f_{i-3}) \end{aligned} \right],$$

where  $\alpha_f = 0.45$  in this study. Other details have been explained in Section 4.3. For temporal algorithm, the third-order TVD Rung-Kutta method is used [22].

Three nonuniform grids are chosen including two seriously deformed ones. Their generations are explained first.

## 5.1 Grid configurations

Three grids are considered: wavy grids, randomized grids and triangular-like grids.

(1) Wavy grids [18].

The grid coordinates are generated by:

$$\begin{cases} x_{i,j} = -\frac{L}{2} + \frac{L}{I_{\max}-1} \left[ (i-1) + A_x \sin \frac{n_{xy}\pi(j-1)}{J_{\max}-1} \right], \\ y_{i,j} = -\frac{L}{2} + \frac{L}{J_{\max}-1} \left[ (j-1) + A_y \sin \frac{n_{xy}\pi(i-1)}{I_{\max}-1} \right], \end{cases}$$

where  $L = 16$ ,  $i = 1, \dots, I_{\max}$ ,  $j = 1, \dots, J_{\max}$ ,  $A_x = 0.4(I_{\max}-1)/L$ ,  $A_y = 0.8(J_{\max}-1)/L$ , and  $n_{xy} = 6$ . Three sets of  $(I_{\max} \times J_{\max})$  are chosen as:  $(41 \times 41)$ ,  $(81 \times 81)$ , and  $(161 \times 161)$ . The  $41 \times 41$  grids is shown in Fig. 1.

(2) Randomized grids [1]

(a) 2-D case

The coordinates are generated by:

$$\begin{cases} x_{i,j} = -\frac{L}{2} + \frac{L}{I_{\max}-1} \left[ (i-1) + 2A_{i,j}(\text{Rand}(0,1) - 0.5)\text{Rand}(0|1) \right], \\ y_{i,j} = -\frac{L}{2} + \frac{L}{J_{\max}-1} \left[ (j-1) + 2A_{i,j}(\text{Rand}(0,1) - 0.5)(1 - \text{Rand}(0|1)) \right], \end{cases}$$

where  $L = 16$ ,  $A_{ij} = 0.45$  at  $i = 5, \dots, I_{\max}-4$  or  $j = 5, \dots, J_{\max}-4$  otherwise  $A_{ij} = 0$ ,  $\text{Rand}(0,1)$  is a random function ranging from 0 to 1 while  $\text{Rand}(0|1)$  is one having the value 0 or 1. Two sets of grid number are chosen as  $(41 \times 41)$  and  $(81 \times 81)$ . The  $41 \times 41$  randomized grids is shown in Fig. 2. It is worthy to mention that the randomized grid here has the largest deformation than that reported in previous literatures [1, 2, 18] with  $A_{ij} = 0.4$ , and further increase of  $A_{ij}$  will cause negative grid-cell area.

(b) 3-D case.

The grid generation is similar to that of 2-D case, which is still generated by randomizing uniform grids with 0.45 magnitude grid spacing in a random direction.

(3) Triangular-like grids.

In order to explore the potential of the proposed methodology, a triangular-like grid is designed to mimic the unstructured grid. The construction is illustrated in Fig. 3. In Fig. 3(a), a series of square cells are built first; then pairs of points collapse into one like

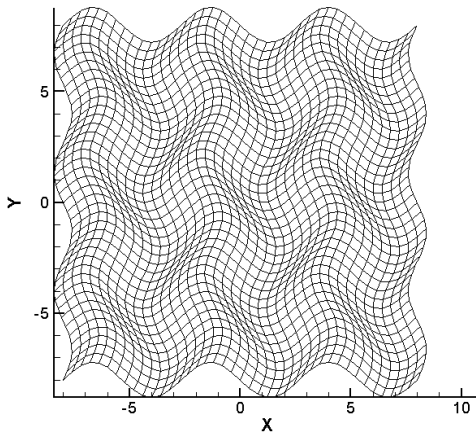


Figure 1:  $41 \times 41$  wavy grids.

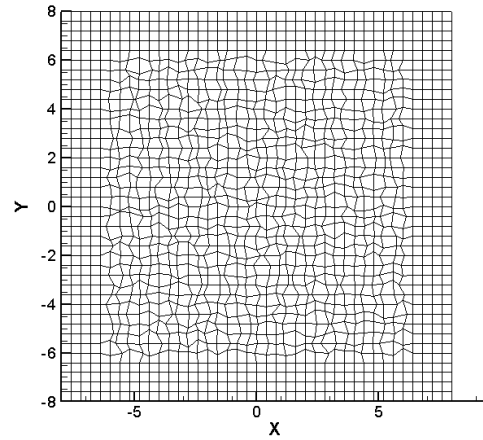
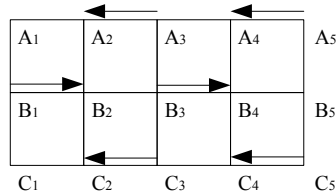
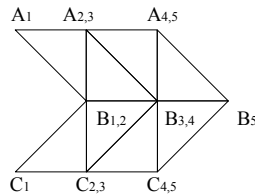


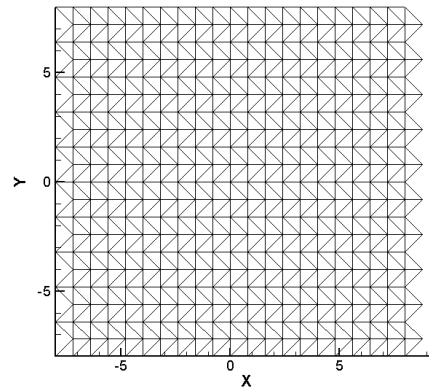
Figure 2:  $41 \times 41$  randomized grids.



(a) before



(b) after



(c)  $41 \times 21$  grids

Figure 3: Generation of the triangular-like grid.

$(A_2, A_3) \rightarrow A_{2,3}$ , while they are still treated as two separate points in the computation. The final grid looks like the one in Fig. 3(b), which resembles typical unstructured topology to some extent.

The computational domain is  $[-8, 8] \times [-8, 8]$ , and two sets of grid number are chosen as  $(41 \times 21)$  and  $(81 \times 41)$ . Fig. 3(c) shows the  $41 \times 21$  grids.

In computations, the periodic boundary condition is employed for all cases, which is realized by extending extra four layers of grids on four sides. To avoid misunderstanding, it is worthy to mention that the choice of largely deformed grids does not indicate the

suggestion of their usage in applications. The tests on such grids are intended to show the capability of proposed methods on extremely difficult cases and provide numerical validations on the conducted analysis.

## 5.2 Check of *FSP* on 3-D $41^3$ randomized grids

Three schemes are first used, i.e., CS4, M-UPW3 and UPW5. A free-stream condition is imposed with the Mach number as 0.5. The computation runs until  $t = 10$  with the time step  $\Delta t = 0.01$ .  $L_2$  errors of velocity component  $v$  and  $w$  are shown in Table 7. In the computation, flux splitting uses the one discussed in Section 3.2.

Table 7:  $L_2$  errors of  $v$  and  $w$ -component in *FSP* test on the randomized grid.

scheme	$v$ -component	$w$ -component
CS4	5.040337010914540E-014	5.048442957102751E-014
M-UPW3	5.450028935790510E-015	5.442990712969394E-015
UPW5	2.421037216639132E-015	2.520031678789157E-015
UPW3(F)+CS6(G)+SW	N/A	N/A

It can be seen from Table 7 that the methodology proposed for the node- and mixed-type upwind schemes are validated to achieve *FSP*. According to the previous discussions, the first CS4 is expected to achieve *FSP* as well, which is also verified by the computation. The result of the fourth method "UPW3(F)+CS6(G) +SW" will be explained later in Section 5.4.

## 5.3 Vortex preservation on three types of grids [1, 18]

This problem is rather popular to investigate the performance of numerical schemes on deformed grids. The flow is non-dimensionalized by the density and the speed of sound, and the free-stream Mach number is 1. An isentropic vortex is initially superimposed on the uniformed flow at  $\vec{r}_0 = (0,0)$  as [18]

$$\begin{cases} (\delta u, \delta v) = \varepsilon \tilde{r} e^{\alpha(1-\tilde{r}^2)} (\sin\theta, -\cos\theta), \\ \delta T = -\frac{(\gamma-1)\varepsilon^2}{4\alpha\gamma} e^{2\alpha(1-\tilde{r}^2)}, \\ \delta S = \delta(p/\rho^\gamma) = 0, \end{cases}$$

where  $\tilde{r} = |\vec{r} - \vec{r}_0|/r_c$ ,  $r_c = 1$ ,  $\alpha = 0.204$ ,  $\varepsilon = 0.3$  and  $\gamma = 1.4$ .

The computation runs from the above initial conditions for a time  $t = 16$  at  $\Delta t = 0.01$ . The period corresponds to one movement circle of the vortex to return to its initial place through the periodic boundary. Three types of meshes are chosen and different schemes are comparatively investigated.

(1) Wavy grids

Three sets of grid numbers are chosen as:  $(41 \times 41)$ ,  $(81 \times 81)$  and  $(161 \times 161)$ . Schemes CS4, M-UPW3 and UPW5 are used in the computation. As a representative, contours of vorticity magnitude on  $41 \times 41$  grids are shown in Fig. 4(a)-(c), and the distribution of  $v$ -component along the line  $j = J_{\max}/2 + 1$  is depicted in Fig. 4(d). The pressure is not chosen for visualization because of its relatively smooth distribution. Although the first three methods achieve  $MI$  and  $FSP$  theoretically, the result of CS4 appears oscillatory due to the lack of dissipation. The quantitative check in Fig. 4(d) shows M-UPW3 and UPW5 demonstrate a reasonable description about the vortex profile, while M-UPW3 behaves more smearing; on the other hand, CS4 yields a result with oscillations with short wave-length at the smooth region away from the vortex. Hence the methodology developed for upwind schemes manifests its advantage over central schemes if additional treatment like filtering is absent.

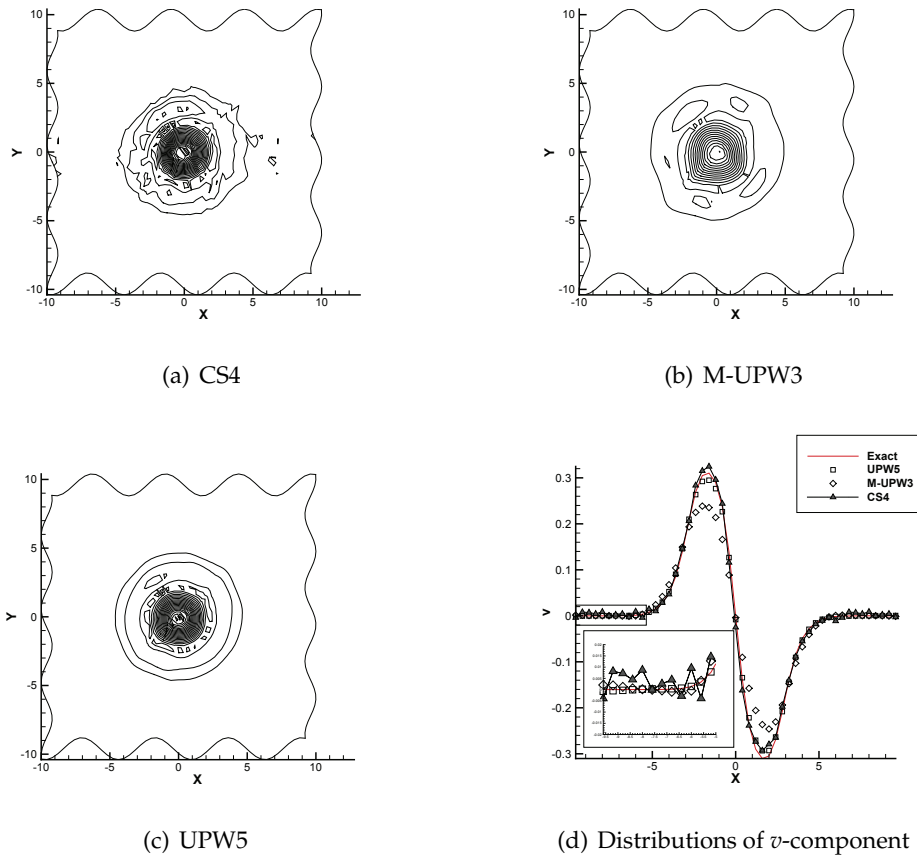


Figure 4: Vorticity contours and  $v$ -distributions along the line at  $j = J_{\max}/2 + 1$  on  $41 \times 41$  wavy grids in moving vortex problem (Contours from 0 to 0.7 with the number 21 in (a)-(c)).

Similar computations are made on the rest two grids and results with the convergence are obtained. Making use of computational errors, the accuracy orders of schemes can be derived and are shown in Table 8. The order of schemes on the wavy grids is smaller than their analytic counterpart, which is consistent with the results in Ref. [18]. The phenomenon might come from the fact that actually wavy grids have nonuniform intervals, while the length scale for computing the order is the constant  $L/I_{\max}$ . The order of CS4 at  $81 \times 81$  grids unexpectedly has a large value, which might be caused by non-convergent behavior during the grid convergence.

Table 8:  $L_2$  errors in the  $v$ -component in moving vortex problem on wavy grids.

Grids	CS4		M-UPW3		UPW5	
	$L_2$ errors	order	$L_2$ errors	order	$L_2$ errors	order
$41 \times 41$	6.839435E-02	–	2.321206E-01	–	4.670484E-02	–
$81 \times 81$	4.818256E-03	3.8273	6.411272E-02	1.85626	3.238539E-03	3.85074
$161 \times 161$	4.213631E-04	3.5154	1.234671E-02	2.37648	1.558367E-04	4.37711

## (2) Randomized grids

Computations are made on two grids with the number ( $41 \times 41$ ) and ( $81 \times 81$ ), where schemes CS4+CF6, W-UPW3 and UPW5 are checked. In this situation, CS4 cannot work independently unless aforementioned sixth-order filter is used. Again, contours of vorticity magnitude on  $41 \times 41$  grids are shown in Fig. 5(a)-(c) and the distribution of  $v$ -component along the line at  $j = J_{\max}/2 + 1$  is depicted in Fig. 5(d). On such seriously deformed grid, two upwind schemes indicate their robustness and fair performance on vortex preservation. Their solutions of  $v$ -component show rather smooth distributions as well, where M-UPW3 appears relatively more dissipative. With the help of filtering, CS4 works normally and generates a result comparable to that of UPW5.

The results on  $81 \times 81$  grids are similar to those on the coarse grid, except for the decreased length scale of irregularities in vorticity contours. Therefore they are omitted for brevity.

At last, the case of vortex preservation in Ref. [23] is tested by UPW5. Initial conditions are almost the same as those mentioned above except that the magnitude of velocity disturbance is " $\varepsilon = 0.02$ " with respect to free-stream sound speed and the randomized level of  $21 \times 21$  grids is 20% in both  $x$  and  $y$  directions. The computation still lasts for one period so that the vortex can return to its initial position through the periodic boundaries. The result of UPW5 is shown in Fig. 6(a) by using contours of vorticity magnitude, and with the courtesy from Ref. [23], the result of so-called WENO-FP in the reference is shown in Fig. 6(b). From the figure, contours of UPW5 show relatively well preservation of concentric symmetry of the vortex and appear more smoothly. In Fig. 6(a), small structures along  $x = 0$  and  $y = 0$  near boundaries are observed, which are suspected to arise from the self-induction of the vortex through periodic condition.

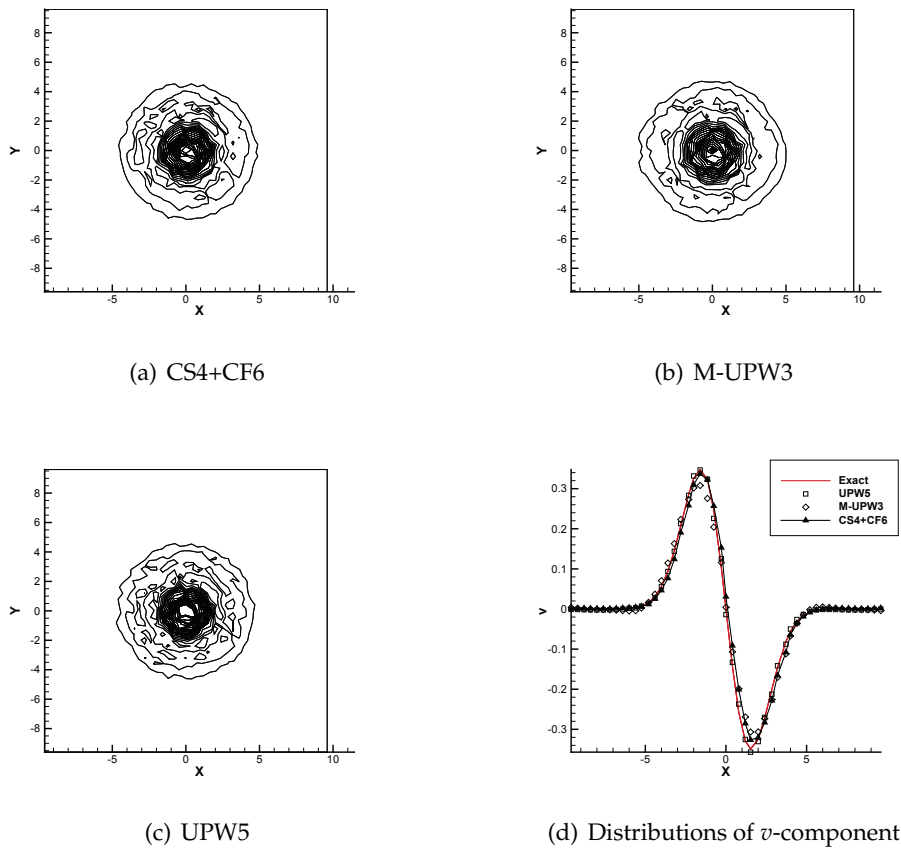


Figure 5: Vorticity contours and  $v$ -distributions along the line at  $j = J_{\max}/2 + 1$  on  $41 \times 41$  randomized grids in moving vortex problem (Contours from 0 to 0.7 with the number 21 in (a)-(c)).

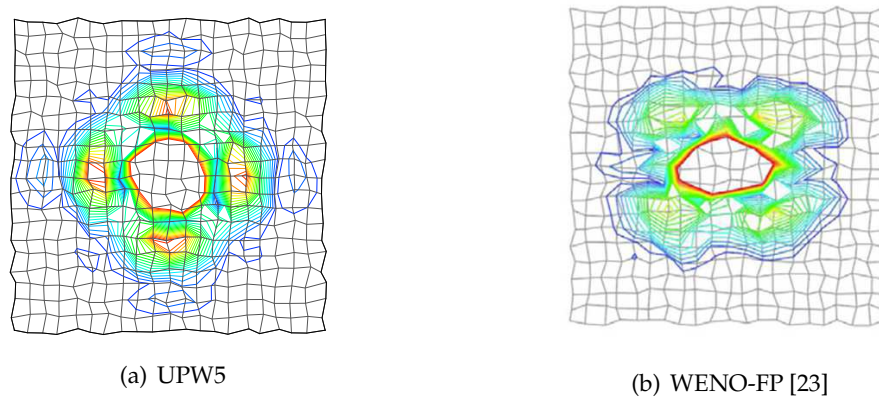


Figure 6: Vorticity contours of different schemes with the courtesy from Ref. [23] (Contours from 0 to 0.005 with number 21).

### (3) Triangular-like grids

Two grid numbers are set as  $(41 \times 21)$  and  $(81 \times 41)$  and three schemes are checked, namely, CS4+CF6, M-UPW3 and UPW5. The individual use of CS4 does not work once more. The vorticity contours on two grids are first shown in Fig. 7, which manifest the

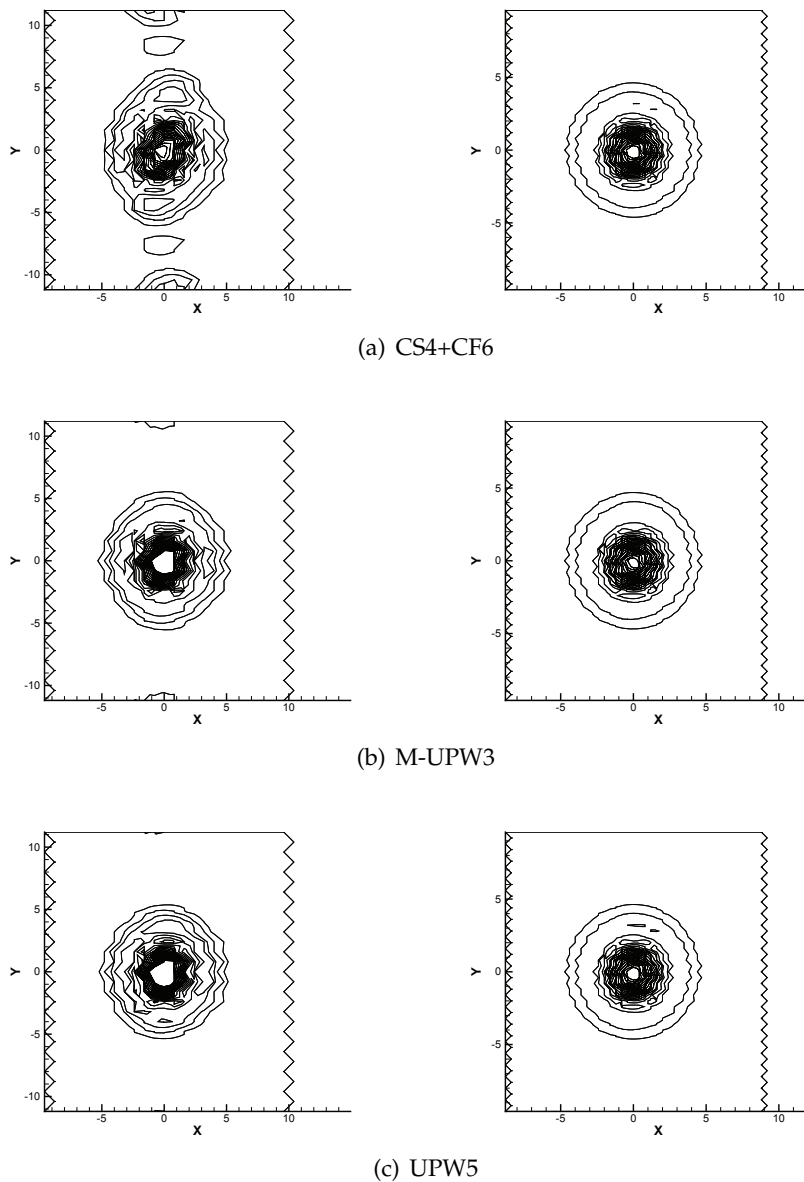


Figure 7: Vorticity contours on  $41 \times 21$  (left) and  $81 \times 41$  (right) triangular-like grids in moving vortex problem (Contours from 0 to 0.7 with number 21).

potential of difference schemes to solve problems on unstructured-like grids if  $MI$  is fulfilled. All contours show more or less oscillations and deviation from the theoretical concentric circles. Such appearance should be caused by the serious grid deformation considering that triangular-like grids differ far from the ideal rectangular ones. It is interesting to observe that on the coarse grid, the vorticity contour by CS4+CF6 appears asymmetric compared with that of M-UPW3 and UPW5. What is more, extra perturbations emerge near the upper and lower boundaries by the central scheme, while upwind schemes yield relatively clean results. When the grid number is increased to  $(81 \times 41)$ , such difference becomes far from obvious because of the convergence to the exact solution.

From a quantitative perspective, distributions of the velocity  $v$ -component on two grids are drawn along the middle horizontal line at  $j = J_{\max}/2 + 1$  in Fig. 8. On the coarse grid, two upwind schemes show a sharper description of  $v$  than that by using CS4+CF6, while the difference becomes less visible as expected when the grid number increases. Considering vorticity contours on  $41 \times 21$  grids in Fig. 7, it seems that upwind schemes indicate a relative better performance than the central scheme with filter on the coarse grid.

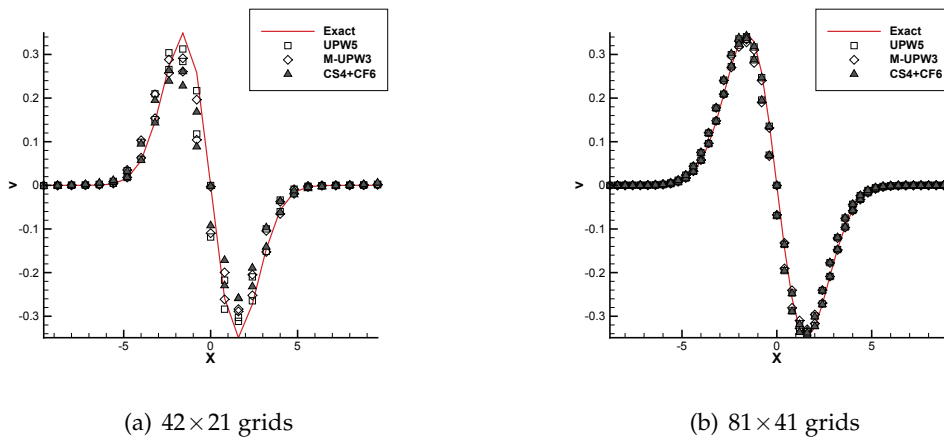


Figure 8: Distributions of  $v$ -component along the line at  $j = J_{\max}/2 + 1$  on triangular-like grids in moving vortex problem.

## 5.4 Discussions

In above, several upwind and central schemes in which metric-evoked errors are carefully disposed are numerically tested. In this part, a set of methods regarding an upwind scheme is tested in free-stream preservation and moving vortex on wavy and randomized grids. The schemes are chosen so that proposed requirement in Section 3 is violated, through which the rationality of current study is further investigated.

The sets of schemes are: (1) The third-order upwind scheme (UPW3) is chosen to discretize the flux derivatives, i.e.,  $(\delta^+ f^+)_i = \frac{(f_{i-2}^+ - 6f_{i-1}^+ + 3f_i^+ + 2f_{i+1}^+)}{6\Delta}$  and so does  $\delta^-$ ; (2) The sixth-order central scheme is chosen to discretize derivatives in grid metrics and Jacobian (see Table 1); (3) Steger-Warming scheme is used for flux splitting. The whole set is abbreviated as "UPW3(F)+CS6(G)+SW". According to previous discussions, the methods violate requirements for upwind scheme to eliminate metric-evoked errors.

First, free-stream preservation on randomized grid is tested, details of which can be found in Section 5.2. After running for several hundred steps at the same  $\Delta t$ , the computation blows up and corresponding  $L_2$  errors are unavailable in Table 6. The result indicates that proposed requirement for upwind scheme is necessary and the importance of previous analysis is testified.

Next, the result of moving vortex on  $41 \times 41$  wavy grids is shown in Fig. 9, and details of the computation can be referred in part (1) Section 5.3. It is surprised to find that "UPW3(F)+CS6(G)+SW" generates a reasonable result, e.g., vorticity contours are relatively smooth, and the distribution of  $v$ -component along the line at  $j = J_{\max}/2 + 1$  resembles that of M-UPW3 in Fig. 4(d). It is conjectured that the acceptable performance of "UPW3(F)+CS6(G)+SW" in this case arise from the not-seriously deformed grid and inherent dissipation of UPW3.

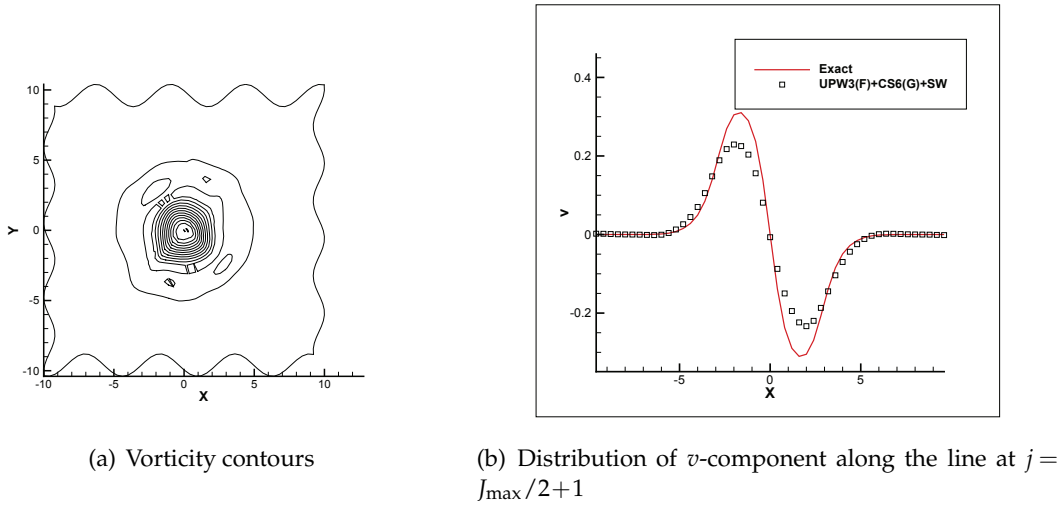


Figure 9: Vorticity contours and  $v$ -distributions of UPW3(F)+CS6(G)+SW on  $41 \times 41$  wavy grids in moving vortex problem (Contours from 0 to 0.7 with the number 21).

At last, the case of moving vortex on  $41 \times 41$  randomized grids is checked, and details of computation can be found in part (2) in Section 5.3. Vorticity contours and  $v$ -component distribution are shown in Fig. 10, where the vortex is completely out of shape and the parametric distributions appear strongly oscillatory. Recalling the result in Fig. 5(c), it is conceivable that large errors are generated from grid metric evaluations,

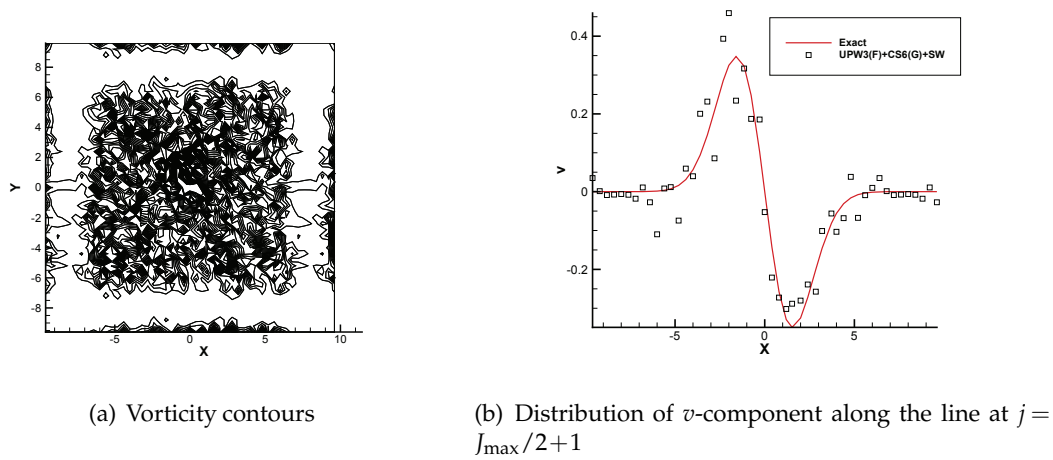


Figure 10: Vorticity contours and  $v$ -distributions of UPW3(F)+CS6(G)+SW on  $41 \times 41$  randomized grids in moving vortex problem (Contours from 0 to 0.7 with the number 21).

and the cause would lie in the violation of requirements for upwind scheme to eliminate metric-evoked errors.

In short, through the above cases by the use of UPW3(F)+CS6(G)+SW, the validity and necessity of proposed requirement for upwind scheme is testified from another point of view.

## 6 Conclusions

The topic to eliminate errors in metric evaluation for arbitrary upwind schemes is investigated with flux splitting being considered. Although linear upwind scheme is known to attain  $MI$  if flux splitting is absent, the splitting is actually indispensable in practical applications and the difficulty is brought in thereby. Brief conclusions are obtained as:

(1) An idea of central scheme decomposition (CSD) is introduced, and the procedure to derive the central scheme  $\delta^{c,(1)}$  is prescribed. The derived  $\delta^{c,(1)}$  is used only for metric evaluations but will not be explicitly used to evaluate flux derivatives, which are still solved by the given linear upwind scheme. Furthermore, the nonlinear extensions of the method mainly aim for half-node- or mixed-type schemes and are supposed to be implemented by nonlinear interpolations. Details in this regard will be different from that in Ref. [23] where nonlinear operations on fluxes were adopted.

(2) Analysis has been made on the requirement of flux splitting to eliminate metric-evoked errors with the satisfaction of the basic relation as  $\hat{E} = \hat{E}^+ + \hat{E}^-$ , and a Lax-Friedrichs-type splitting scheme is proposed as a concrete example to combine with the upwind scheme.

(3) The above methods and the metric forms derived by Thomas, Lombard and Neier [6,7] can directly be applied for arbitrary upwind node-type schemes. For half-node- or mixed-type scheme, interpolations should additionally be used to derive variables at half nodes. After analyzing the requirements to achieve *MI*, an idea of directionally consistent interpolation is proposed and should be followed in implementations, otherwise *MI* may still be violated.

The problems of *FSP* and moving vortex preservation are chosen for numerical validations. Three deformed grids are used, i.e., wavy grids, seriously randomized grids and triangular-like grids. Numerical results validate the theoretical outcomes, and the capability of upwind schemes on largely deformed grids is manifested.

## Acknowledgments

This work is sponsored by the National Science Foundation of China under the Grant Number 11272037 and 91541105, and is also partially supported by National Key Basic Research and Development 973 Program of China under Grant Number 2014CB744100.

## Appendix

This appendix briefly reviews the proof of numerical commutativity of mixed derivative by Vinokur and Yee [8]. Before further discussion, the tensor or Kronecker product of two arbitrary matrices  $A$  and  $B$  is introduced first, which yields a block matrix with the element:  $(A \otimes B)_{ij} = A_{ij}B$ . Based on the concept, the mixed product rule exists [8] for two pairs of conformable matrices  $\{A, C\}$  and  $\{B, D\}$  as

$$(A \otimes B)(C \otimes D) = AC \otimes BD, \quad (\text{A.1})$$

where  $AC$  denotes ordinary matrix product. Then consider the 3-D curvilinear coordinates system with the dimension  $(l, m, n)$  in  $(\xi, \eta, \zeta)$  directions. Take  $\xi$  direction as an example. Suppose the difference scheme for  $u_\xi$  can generally be expressed as  $A^\xi u_\xi = B^\xi u$ , where  $A^\xi$  and  $B^\xi$  are  $l$  by  $l$  matrices, and  $u_\xi$  and  $u$  are  $l$ -dimensional vectors. Assuming the computational order for the whole discrete variables is in the sequence of  $\xi, \eta$  and  $\zeta$ , then the equation for all  $u_\xi$  can be written as  $\bar{A}^\xi \bar{u}_\xi = \bar{B}^\xi \bar{u}$ , where  $\bar{u}$  and  $\bar{u}_\xi$  are  $l \times m \times n$ -dimensional vectors of  $u$  and  $u_\xi$ ,  $\bar{A}^\xi$  and  $\bar{B}^\xi$  and are  $(l \times m \times n)$  by  $(l \times m \times n)$  matrices with the form

$$\begin{cases} \bar{A}^\xi = I^n \otimes (I^m \otimes A^\xi), \\ \bar{B}^\xi = I^n \otimes (I^m \otimes B^\xi). \end{cases} \quad (\text{A.2})$$

In Eq. (A.2),  $I^n$  is  $n$  by  $n$  identity matrix and so is with  $I^m$ . In the same way, the equation for all  $u_\eta$  can be written as  $\bar{A}^\eta \bar{u}_\eta = \bar{B}^\eta \bar{u}$ , where

$$\begin{cases} \bar{A}^\eta = I^n \otimes (A^\eta \otimes I^l), \\ \bar{B}^\eta = I^n \otimes (B^\eta \otimes I^l). \end{cases} \quad (\text{A.3})$$

Then the discretization of the mixed derivative  $u_{\xi\eta}$  becomes:  $\bar{A}^\eta(\bar{A}^\xi u_\xi)_\eta = \bar{A}^\eta \bar{A}^\xi \bar{u}_{\xi\eta} = \bar{B}^\eta \bar{B}^\xi \bar{u}$ . Using Eq. (A.1),  $\bar{A}^\eta \bar{A}^\xi = [I^n \otimes (A^\eta \otimes I^l)] [I^n \otimes (I^m \otimes A^\xi)] = I^n \otimes [(A^\eta \otimes I^l)(I^m \otimes A^\xi)] = I^n \otimes A^\eta \otimes A^\xi$ . In the same manner,  $\bar{A}^\xi \bar{A}^\eta = I^n \otimes A^\eta \otimes A^\xi$ , and therefore  $\bar{A}^\eta \bar{A}^\xi = \bar{A}^\xi \bar{A}^\eta$ . Similarly,  $\bar{B}^\eta \bar{B}^\xi = \bar{B}^\xi \bar{B}^\eta$ . Hence,  $\bar{u}_{\xi\eta} = \bar{u}_{\eta\xi}$  or the numerical commutativity is satisfied. In a similar way,  $\bar{u}_{\xi\xi} = \bar{u}_{\xi\xi}$  and  $\bar{u}_{\eta\xi} = \bar{u}_{\xi\eta}$  can be established. More details are suggested to Ref. [8].

## References

- [1] M. R. Visbal and D. V. Gaitonde, On the use of high-order finite-difference schemes on curvilinear and deforming meshes, *J. Comput. Phys.*, 181(2002): 155-195.
- [2] T. Nonomura, N. Iizuka, K. Fujii, Freestream and vortex preservation properties of high-order WENO and WCNS on curvilinear grids, *Computers and Fluids* 39(2010): 197-214.
- [3] M. Vinokur, Conservative Equations of Gasdynamics in Curvilinear Coordinate Systems, *J. Comput. Phys.*, 14(1974): 105-125.
- [4] T. H. Pulliam and J. L. Steger, On implicit finite-difference simulations of three dimensional flow, *AIAA* 1978-10.
- [5] P. D. Thomas and C. K. Lombard, The Geometric Conservation Law-A Link Between Finite-Difference and Finite-Volume Methods of Flow Computation on Moving Grids, *AIAA* 1978-1208.
- [6] P. D. Thomas and C. K. Lombard. Geometric Conservation Law and Its Application to Flow Computations on Moving Grids, *AIAA J.*, 1979, 17(10): 1030-1037.
- [7] P. D. Thomas and K. L. Neier, Navier-Stokes Simulation of Three-Dimensional Hypersonic Equilibrium Flows with Ablation, *J. Spacecraft and rocket*, 1990, 27(2): 143-149.
- [8] M. Vinokur and H. C. Yee, Extension of efficient low dissipation high order schemes for -3D curvilinear moving grids, *NASA Technical Memorandum* 209598, 2000.
- [9] J. F. Thompson, Z. U. A. Warsi, and C. W. Mastin, *Numerical grid generation*, Elsevier Science Publishing, 1985.
- [10] D. V. Gaitonde and M. R. Visbal, Further development of a Navier-Stokes solution procedure based on high-order formulas, *AIAA* 1999-0557.
- [11] X. Deng, M. Mao, G. Tu, H. Liu, H. Zhang, Geometric conservation law and applications to high-order finite difference schemes with stationary grids, *J. Comput. Phys.*, 230(2011): 1100-1115.
- [12] X. Deng, Y. Min, M. Mao, H. Liu, G. Tu, H. Zhang, Further studies on geometric conservation law and applications to high-order finite difference schemes with stationary grids, *J. Comput. Phys.*, 239(2013): 90-111.
- [13] Y. Abe, N. Iizuka, T. Nonomura, K. Fujii, Symmetric-conservative metric evaluations for higher-order finite difference scheme with the GCL identities on three-dimensional moving and deforming mesh, *ICCFD7-2012-280*.
- [14] Y. Abe, T. Nonomura, N. Iizuka, K. Fujii, Geometric interpretations and spatial symmetry property of metrics in the conservative form for high-order finite-differences schemes on moving and deforming grids, *J. Comput. Phys.*, 260(2014): 163-203.
- [15] M. Vinokur, An analysis of finite-difference and finite-volume formulations of conservation laws, *J. Comput. Phys.*, 81(1989): 1-52.
- [16] X. Cai and F. Ladeinde, Performance of WENO Scheme in Generalized Curvilinear Coordinate Systems, *AIAA* 2008-36.

- [17] S. K. Lele, Compact Finite Difference Schemes with Spectral-like Resolution, *J. Comput. Phys.*, 103(1992): 16-42.
- [18] Y. Jiang, C. Shu, and M. Zhang, Free-stream preserving finite difference schemes on curvilinear meshes, *Methods and Applications of Analysis*, 2014, 21(1): 001-030.
- [19] Y. Abe, N. Lizuka, T. Nonmura, K. Fujii, Symmetric-conservative metric evaluations for high-order finite difference scheme with the GCL identities on three-dimensional moving and deforming mesh, *Seventh International Conference on Computational fluid Dynamics*, ICCFD7-2801, 2012.
- [20] H. Zhang, Some important problems for high order accurate difference scheme solving gas dynamic equations, *Acta Aerodynamica Sinica*, 11(1993): 347-356.(in Chinese)
- [21] D. V. Gaitonde and M. R. Visbal, High-order schemes for Navier-Stokes equations: algorithm and implementation into FDL3DI, AFRL-VA-WP-TR-1998-3060, 1998.
- [22] C. W. Shu, High order weighted essentially nonoscillatory schemes for convection dominated problems, *SIAM review*, 2009, 51(1): 82-126.
- [23] T. Nonomura, D. Terakado, Y. Abe, K. Fujii, A new technique for freestream preservation of finite-difference WENO on curvilinear grid, *Computers and Fluids*, 107(2015): 242-255.